

Merging modelled and reported flood impacts in Europe in a combined flood event catalogue, 1950-2020

Dominik Paprotny¹, Belinda Rhein^{1,2}, Michalis I. Voudoukas³, Paweł Terefenko⁴, Francesco Dottori⁵, Simon Treu¹, Jakub Śledziowski⁴, Luc Feyen⁶, and Heidi Kreibich⁷

¹ Potsdam Institute for Climate Impact Research (PIK), Member of the Leibniz Association, P.O. Box 60 12 03, 14412 Potsdam, Germany, ² Humboldt-Universität zu Berlin, Berlin, Germany, ³ University of the Aegean, Department of Marine Sciences, Mytilene, Greece, ⁴ Institute of Marine and Environmental Sciences, University of Szczecin, Adama Mickiewicza 16, 70-383 Szczecin, Poland, ⁵ CIMA Research Foundation, Savona, Italy, ⁶ European Commission, Joint Research Centre (JRC), Ispra, Italy, ⁷ GFZ German Research Centre for Geosciences, Section Hydrology, Potsdam, Germany
Correspondence to: Dominik Paprotny (dominik.paprotny@pik-potsdam.de)

Abstract. Long-term trends in flood losses are regulated by multiple factors including climate variation, demographic dynamics, economic growth, land-use transitions, reservoir construction and flood risk reduction measures. Attribution of those drivers through the use of counterfactual scenarios of hazard, exposure or vulnerability first requires a good representation of historical events, including their location, intensity and the factual circumstances in which they occurred. Here, we develop a chain of models that is capable of recreating riverine, coastal and compound floods in Europe between 1950 and 2020 that had a potential to cause significant socioeconomic impacts. This factual catalogue of almost 15,000 such events was scrutinised with historical records of flood impacts. We found that at least 10% of them had led to significant socioeconomic impacts (including fatalities) according to available sources. The model chain was able to capture events responsible for 96% of known impacts contained in the HANZE flood impact database in terms of persons affected and economic losses, and for 81% of fatalities. The dataset enables studying drivers of vulnerability and flood adaptation due to a large sample of events with historical impact data. The model chain can further be used to generate counterfactual events, especially related to climate change and human influence on catchments.

1 Introduction

Flood risk is constantly evolving and influenced by a wide array of drivers, related to atmospheric, land surface and socio-economic processes (Merz et al., 2021). Recent decades have been identified as a particularly flood-rich period along European rivers (Blöschl et al., 2020) and increasing sea levels are expected to exacerbate coastal flood risk (Voudoukas et al., 2017, 2023, Nicholls et al., 2021). At the same time exposure is growing rapidly (Paprotny et al., 2018b, [Andreadis et al., 2022](#), Rentschler et al., 2023) and mitigation actions are implemented in reaction to floods (Kreibich et al., 2022). Disentangling the different risk drivers requires considerable modelling effort to reconstruct the factual circumstances surrounding the occurrence

31 of floods and modelling them again under alternative (counterfactual) conditions (Scussolini et al., 2023). Such analyses enable
32 impact attribution, i.e. linking changes in impacts with their likely causes. It can then provide information on long-term
33 development of risk, which in turn has implications on cost-benefit analyses or risk management planning (Kreibich et al.,
34 2019).

35 The recent Sixth Assessment Report of the Intergovernmental Panel on Climate Change, in the chapter on Europe (Bednar-
36 Friedl et al., 2022), indicated low confidence in trends in riverine and coastal flood impacts in the past half-century, even if
37 some increase was detected for parts of the continent. The report contained very limited information on attribution, but this
38 gap is being slowly filled by new studies. For example, Sauer et al. (2021) quantified hazard, exposure and vulnerability
39 changes for flood events globally, finding that for Europe the increase in flood losses was driven almost entirely by exposure,
40 with some small decline in hazard and vulnerability. Though the timeframe of the study was short (1980–2010), it highlighted
41 the role of exposure similarly to Paprotny et al. (2018b), who presented exposure-adjusted losses for 1870–2016 (with
42 consideration for gaps in flood impact reporting), finding no upward trend in economic losses and a strong decline in fatalities.
43 Long-run global data on climatic and socioeconomic drivers under factual and counterfactual scenarios are available from the
44 Inter-Sectoral Model Intercomparison Project, or ISIMIP 3a (Frieler et al., 2024), but they mostly have coarse resolution that
45 is not easily applicable to Europe and have not yet been used for flood impact attribution. Impact attribution of European
46 floods was also carried out with a case study-based, semi-quantitative approach of comparing “paired events”, i.e. floods that
47 have occurred in the same area some years apart (Kreibich et al., 2023). This approach has an advantage mainly in the context
48 of drawing practical conclusions for flood adaptation (Kreibich et al., 2019). Studies that derived projections of future flood
49 risk in Europe have indicated that all three components of risk play an important role in determining changes in the impact
50 magnitude (Rojas et al., 2013, Vousdoukas et al., 2018, Steinhilber et al., 2022, Schoppa et al., 2024).

51 Particular effort is needed in reconstructing the intensity and spatial footprint of flood events. For instance, the loss-
52 normalisation study of Paprotny et al. (2018b) used 100-year riverine and coastal flood hazard maps as proxies for impact
53 zones within subnational regions indicated as affected in the HANZE database (Paprotny et al., 2018a). This approach did not
54 include the effect of climate change, human influence on catchments or simply the variation in return period of different events.
55 There have been attempts to reconstruct past river floods for North America (Wing et al., 2021) or storm surge footprints
56 globally (Enríquez et al., 2020), but none specifically for Europe. Satellite-derived flood footprints can also be linked to impact
57 records, as in Mester et al. (2023), but such datasets cover only a short timeframe and do not resolve the problem of generating
58 a counterfactual hazard scenario.

59 In this study we develop a modelling chain to generate a factual flood catalogue for 42 European countries covering the period
60 1950–2020, which could be further used to run counterfactual scenarios. We only cover the factual scenarios and focus on
61 deriving the best possible reconstruction of past riverine, coastal and compound floods. The main metric of success of the
62 modelling chain is its ability to correctly derive the time, location and intensity of 2037 actual floods contained in the HANZE
63 flood impact database (Paprotny et al., 2023). We further aim at deriving not only the floods that caused significant

64 socioeconomic impacts, but also those that did not happen despite their hydrological extremity due to existing flood protection,
65 as this could later be used to quantify the level of European flood protection.

66 Thanks to the availability of new high-resolution estimates of past population and economic exposure (Paprotny and Mengel,
67 2023), we narrow down our catalogue of floods only to those with significant socioeconomic impact potential, rather than
68 those which were extreme only from a hydrological perspective. This enables comparison with historical records of flood
69 impacts and classifying the modelled events in accordance to their real-life consequences (or lack thereof). Finally, the focus
70 is on coastal, compound and slow-onset riverine flooding. Flash flood events occurring in small catchments (i.e. with an
71 upstream area below 100 km²) are not considered in our analysis due to the insufficient resolution of the riverine flood models
72 available for Europe. Furthermore, we explicitly omit urban floods resulting from insufficient storm drainage rather than from
73 channel overflow.

74 The paper provides a short method overview in section 2.1, which is followed by details on the coastal (2.2) and riverine (2.3)
75 components of the modelling chain, which are brought together for a final flood catalogue compared with historical records
76 (2.4). Validation of the hydrological hazard follows in the next sections (2.5, 3.1), with an overview of risk indicators derived
77 from the catalogue (3.2) and finally comparison between modelled and observed flood impacts (3.3). The discussion analyses
78 the limitations and uncertainties of both the modelled (4.1) and observational data (4.2), before drawing conclusions and
79 highlighting possible applications of the flood catalogue (section 5).

80 **2 Methods**

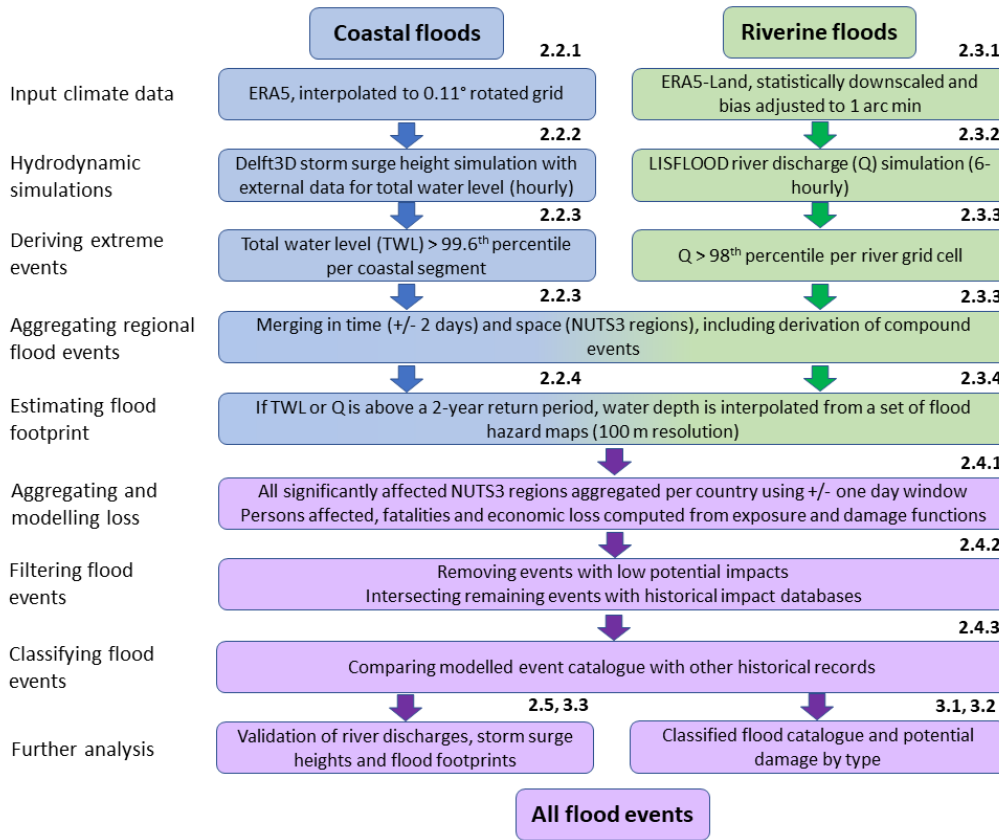
81 **2.1 Overview**

82 Simulating riverine and coastal floods requires different modelling approaches. First, we derive extreme river discharges and
83 coastal water levels, then we apply a common approach to produce flood intensity maps, compute damages, and aggregate
84 the results spatiotemporally. Compound floods are generated by combining the results of the two strands of modelling work,
85 therefore we run the coastal model first, and compound floods are considered as part of the riverine component, drawing on
86 the previous coastal results. The methodology is briefly summarised in [Table Fig. 1](#).

87

Table 1. Summary of the methodology, sections with the corresponding descriptions are given in square brackets.

Step	Coastal floods	Riverine floods
Input climate data	ERA5, interpolated to 0.11° rotated grid [2.2.1]	ERA5-Land, statistically downscaled and bias adjusted to 1 arc min [2.3.1]
Hydrodynamic simulations	Delft3D storm surge height simulation with external data for total water level (hourly) [2.2.2]	LISFLOOD river discharge (Q) simulation (6-hourly) [2.3.2]
Deriving extreme events	TWL > 99.6 th percentile per coastal segment [2.2.3]	Q > 98 th percentile per river grid cell [2.3.3]
	Merging in time (+/- 2 days) and space (NUTS3 regions), including derivation of compound events [2.2.3, 2.3.3]	
Estimating flood footprint	If TWL/Q > 2-year return period, water depth interpolated from a set of flood hazard maps (100 m resolution) [2.2.4, 2.3.4]	
Aggregating flood events	All significantly affected NUTS3 regions aggregated per country using +/- one day window [2.4.1]	
Potential loss modelling	Persons affected, fatalities and economic loss computed from 100-m exposure grid and damage functions [2.4.1]	
Filtering and analysis of flood events	Removing events with low potential impacts	
	Intersecting remaining events with historical impact databases [2.4.2]	
	Comparing modelled event catalogue with other historical records [2.4.3]	
Validation	River discharges, storm surge heights and flood footprints [2.5, 3.1]	
Further analysis	See sections 3.2 and 3.3	



90

91 [Figure 1. Workflow of the methodology, with section numbers indicated above each box.](#)

92

93 In [Table-Fig. 1](#), the aggregation of extreme discharge or water levels spatially by using NUTS3 regions is mentioned. This
 94 refers to the European Union’s (EU) Nomenclature of Territorial Units for Statistics (NUTS). This classification has 4 levels
 95 (0, 1, 2, 3), in which 0 is the national level and 3 is the finest sub-regional division. NUTS3 regions are usually administrative
 96 divisions, though at times statistical (analytical) regions are used instead, by amalgamating smaller administrative units
 97 (Eurostat, 2022). Due to its relevance for determining regional policy, data dissemination, and socioeconomic analyses in the
 98 EU, we use this classification as our principal unit of analysis. This further enables direct comparison with the HANZE flood
 99 impact catalogue, which contains data on 2037 reported floods in the study area since 1950, including footprints defined at
 100 NUTS3 level (Paprotny et al., 2023). HANZE also includes exposure and other subnational statistics at the same resolution
 101 (Paprotny and Mengel, 2023). The generation of a high-resolution boundary map of 1422 NUTS3 regions, version 2010, or
 102 their equivalents, is described in Paprotny and Mengel (2023). We further aggregate flood events at national level for
 103 comparison with reported impacts, as this is the typical resolution in which such information is provided. Consequently, the

104 catalogue is not specific for river catchments or sea basins (as in e.g. Diederer et al., 2019), but for countries and their
105 subdivisions.

106 It should be highlighted that the catalogue represents possible floods without considering structural flood protection measures,
107 hence they are not included in the potential flood footprint estimates. Due to the very limited information on present or past
108 protection standards, adding estimates of those would potentially create large inaccuracies by filtering out events that happened
109 in history.

110 **2.2 Coastal model**

111 **2.2.1 Climate data**

112 We model storm surge heights driven by hourly 10-m wind speeds (u and v component) and surface air pressure, drawing data
113 from the latest ERA5 climate reanalysis (Hersbach et al., 2020). The data were downloaded at a resolution of 0.25°
114 (approximately 28 km at the equator) and then interpolated using first-order conservative remapping (Jones, 1999) to a 0.11°
115 rotated-pole (12.5 km) grid used in our storm surge model, which in turn is the same as the CORDEX grid used in European
116 climate projections (Jacob et al., 2014). Apart from the interpolation, no further adjustments were made to the data.

117 **2.2.2 Sea level estimation**

118 The principal component of extreme sea levels are storm surges, which we estimate through a continuous simulation in
119 Delft3D. This hydrodynamic model is commonly applied in continental- or global-scale surge modelling (e.g. Vousdoukas et
120 al., 2016a, Ganguli et al., 2020, Muis et al., 2020). The model set-up is the same as described in Paprotny et al. (2016, 2019),
121 with the difference that it is forced by wind and atmospheric pressure fields from ERA5 instead of ERA-Interim. We also
122 carried out a calibration, using the previous calibration as the starting point, by adjusting the sea bottom roughness coefficients
123 for different basins around Europe, and comparing the modelled surge heights with tide gauge observations for years 2011–
124 2019. This recalibration also benefited from much better availability of observational data, which are described in section 2.5,
125 as they are also used to validate the final simulation. Additionally, the timestep of the model was reduced to 15 min, with
126 outputs saved hourly, compared to 30 min and 6 hours, respectively, in the original version. The model was run from 1 January
127 1949 [to 31 December 2020](#), with the first year used only as spin-up. Actual ERA5 data was used in the spin-up phase thanks
128 to recent extension of the dataset to 1940.

129 As storm surge heights are only one component of extreme sea levels, the hourly total water level (L) is the combination of six
130 components:

$$131 \quad L = S + T + W + D + M + G \quad (1)$$

132 Where:

- 133 • S is the hourly storm surge height;

- T is the hourly tide elevation, computed with pyTMD package (<https://github.com/tsutterley/pyTMD>) from 34 tidal constituents;
- W is the hourly wave run-up, assumed to be 20% of significant wave height (recommended by U.S. Army Corps of Engineers, 2002, used e.g. in Vousdoukas et al., 2016b);
- D is the mean dynamic topography defined as the average sea surface height for 1993–2012 above geoid;
- M is the long-term variation in sea level related to climatic variation (“sea level rise”, SLR), defined as average annual difference from average sea level in year 2000;
- G is the glacial isostatic adjustment (GIA) computed from long-term historical rate of change.

Each component was derived from a different source, as summarised in Table 2.1.

Table 2.1. Source of data for computing hourly total water level. * coarser global data were used for northernmost coasts of Europe

Component	Source	Spatial resolution	Temporal resolution	Reference
Storm surge height	Delft3D simulation (this study)	12.5 km	hourly	Paprotny et al. (2016)
Tide elevation	FES2014	1/16°	hourly	Lyard et al. (2021)
Wave run-up	ERA5	1/2°	hourly	Hersbach et al. (2020)
Mean dynamic topography	Global Ocean Mean Dynamic Topography (combines global CNES-CLS18 and CMEMS2020 for Black and Mediterranean seas)	1/8°	1993-2012 average	Mulet et al. (2021)
Sea level rise	1950–99: Hourly Coastal water levels with Counterfactual (HCC)	10 km	hourly (used as annual average)	Treu et al. (2023, 2024)
	2000–2020: European Seas Gridded L4 Sea Surface Heights*	1/8°	monthly (used as annual average)	Taburet et al. (2019)
	2000–2020: Global Ocean Gridded L4 Sea Surface Heights*	1/4°	monthly (used as annual average)	Pujol et al. (2016)
Glacial isostatic adjustment	ICE-6G_C	1/5°	long-term rate of change	Argus et al. (2014), Peltier et al. (2015)

2.2.3 Extracting coastal flood events

As the resolution of each dataset that is used to derive the total water level varies, we assign the nearest grid point of each model to 5884 coastal segments defined in the coastal flood hazard model (Vousdoukas et al., 2016b) with a nearest-neighbour approach. [The segments represent no more than 25 km of the coast \(if completely straight\), but usually about 15 km. They stretch up to 100 km inland, but far less for more complex areas such as deltas, estuaries, fjords, or islands.](#) From the detrended (1950–2020) hourly timeseries, occurrences of water level above the 99.6th percentile were identified and considered potential coastal floods. [The detrending was needed as events derived here are used for extreme value analysis \(section 2.2.4\).](#) Occurrence of water levels below the 99.6th percentile for at least two full calendar days separated two events from each other. Such thresholds lead to, on average, about five potential flood events per year. Then, events were aggregated according to

155 NUTS3 regional boundaries, again with the principle that the beginning of any segment-level flood event in a NUTS3 region
156 has to occur at least two full calendar days after the end of any previous segment-level event in that region.

157 **2.2.4 Deriving coastal flood footprints**

158 For each coastal segment in the dataset, an extreme value analysis was carried out using a Generalised Pareto distribution and
159 a peak-over-threshold approach. [The analysis was carried out with Matlab function *fitdist*, using maximum likelihood
160 estimation and the 99.6th percentile thresholds from the previous step.](#) This enabled deriving extreme sea level scenarios (return
161 periods of 2, 5, 10, 20, 30, 50, 100, 200, and 500 years) for coastal inundation modelling. This was carried out according to a
162 methodology developed by Vousdoukas et al. (2016b). Briefly, the maps were generated with the Lisflood-ACC (LFP) model
163 (Bates et al., 2010) applied at 30 m spatial resolution. In terms of Digital Elevation Model (DEM), we use the recently published
164 GLO-30 DEM (European Space Agency and Sinergise, 2021) after applying post-processing using global LIDAR observations
165 to further remove vertical bias, correcting for buildings and vegetation. The description of the GLO-30 post-processing is
166 described in detail in Pronk et al. (2023, 2024). The simulations consider gridded hydraulic roughness values derived from land-
167 use maps (Zanaga et al., 2021). Lisflood-ACC is applied for each coastal segment with the model domain extending up to 200
168 km landwards in order to ensure the inclusion of all potentially hydrologically connected areas that may lie inland and away
169 from the coast.

170 Total water level of each segment-level flood event is linked with the water level used to generate the flood hazard maps for
171 each segment. In this way, it is possible to interpolate water depths from the stack of hazard maps to event-specific extreme
172 sea levels. This is only done if the water levels for an event exceed a flood threshold, defined as the higher of the two following
173 thresholds:

- 174 • Total water level with a 2-year return period, derived from the Generalised Pareto distribution;
- 175 • Maximum observed total water level minus storm surge height.

176 The first threshold was chosen for consistency with the riverine model as it is akin to the typical definition of a bank-full river
177 discharge. The second threshold was added to avoid overestimating risk in regions (mainly Eastern Mediterranean), where
178 storm surge heights are very low, but wave run-up contributes significantly to extreme sea level.

179 Only grid cells with water depths of at least 10 cm were considered inundated for consistency with riverine flood maps. The
180 individual flood maps for each coastal segment were aggregated within a NUTS3-level event. Finally, only those NUTS3-
181 level events were preserved for further analysis if the potential flood zone was at least 100 ha. As further processing is carried
182 out together with the riverine model, we now describe the river component, and continue explaining the next steps towards the
183 combined flood catalogue in section 2.4.

184 **2.3 Riverine model**

185 **2.3.1 Climate data**

186 We used river discharge from Tilloy et al. (2024) that was modelled using ERA5-Land, which is a downscaled version of
187 ERA5 characterised by 0.1° (approximately 11 km at the equator) resolution (Muñoz-Sabater et al., 2021). It was further
188 statistically downscaled and bias adjusted to 1' (arc minute) resolution using ISIMIP3BASD v3.0.0 method developed by
189 Lange (2019, 2022), using EMO-1 gridded observational data, which is a 1' variant of the EMO-5 dataset developed by
190 Thiemiig et al. (2022). Temperature and precipitation with 6-hourly resolution were used as the primary driver of the
191 hydrological model, while potential evapotranspiration was computed at daily resolution using the LISVAP model by van der
192 Knijff (2006). For details on the preparation of the meteorological data, we refer to Tilloy et al. (2024).

193 **2.3.2 River discharge simulation**

194 [Tilloy et al. \(2024\)](#) ~~River discharges were~~ modelled [river discharges a](#) through continuous simulations using the LISFLOOD
195 hydrological model (Burek et al., 2013) implemented in the European Flood Awareness System, or EFAS (Copernicus
196 Emergency Management Service, 2023). Tilloy et al. (2024) used the latest model set-up, v5.0 (Choulga et al., 2023), and
197 simulated river discharges with meteorological inputs described in section 2.3.1. The EFAS model was run ~~starting from 3~~
198 January 1950 [to 31 December 2020](#) following the 71-year pre-run. Due to rapid evolution of socioeconomic conditions in the
199 catchments of Europe, the input socioeconomic maps were changed with the start of every new calendar year of the simulation.
200 The evolving socioeconomic conditions included land use (in six classes), reservoirs (based on the year of construction of each
201 dam), and water demand (in four sectors). For details on the river discharge simulation and its validation, we again refer to
202 Tilloy et al. (2024).

203 **2.3.3 Extracting riverine flood events**

204 [From Tilloy et al. \(2024\)](#) ~~The output of the river model is~~ [we derived](#) a time series of 6-hourly discharge for 7.5 million grid
205 cells. Due to the availability of flood hazard maps for footprint estimation (section 2.3.4), we extract data only for 282,528
206 grid cells that have an upstream area of at least 100 km². Occurrences of discharge above the 98th percentile (on annual basis)
207 were identified and considered potential riverine floods. Occurrence of water levels below the 98th percentile for at least two
208 full calendar days separated two events from each other. As in the coastal model (section 2.2.3), those thresholds were intended
209 to produce roughly five potential flood events per year in each grid cell. Then, events were aggregated according to NUTS3
210 regional boundaries, again with the principle that the beginning of any grid cell-level flood event in a NUTS3 region has to
211 occur at least two full calendar days after the end of any previous grid cell-level event in that region.

212 **2.3.4 Deriving riverine and compound flood footprints**

213 For each grid cell in the dataset, an extreme value analysis was carried out using a Generalised Pareto distribution and a peak-
214 over-threshold approach, where the peak discharge was detrended based on annual maximum discharge for 1950–2020. [The](#)
215 [analysis was carried with Python package SciPy, using maximum likelihood estimation and the 98th percentile thresholds from](#)
216 [the previous step.](#) In contrast to the coastal model (section 2.2.4), no additional hydrodynamic modelling was carried out in
217 the riverine model. Instead, the flooding processes were represented using the dataset of flood hazard maps developed by
218 Dottori et al. (2022), which are available for a range of return periods from 10 to 500 years for grid cells with an upstream area
219 above 500 km². The maps were generated with the Lisflood-ACC (LFP) model (Bates et al., 2010), applied at 100 m spatial
220 resolution and driven by hydrological simulations from a previous set-up of EFAS (Arnal et al., 2019). In this study, given the
221 different resolutions of the LISFLOOD simulations and the flood hazard maps, the two datasets were matched according to
222 the procedure described in Dottori et al. (2022).

223 To provide coverage for smaller catchments, the flood maps by Paprotny et al. (2017) were applied for grid cells with an
224 upstream area of 100–499 km². The maps for five scenarios (return periods of 10, 30, 100, 300 and 1000 years) were based on
225 discharges estimated with a Bayesian Network-based model from Paprotny and Morales-Nápoles (2017). The simulations
226 were performed using a one-dimensional ‘steady-state’ hydraulic model Deltares SOBEK to obtain water levels along rivers.
227 Those levels were then used to generate water depth maps over a digital elevation model. The maps use the exact same grid as
228 the ones from Dottori et al. (2022). For details on the methodology and validation of the maps we refer to Paprotny et al.
229 (2017).

230 Peak river discharge per each grid cell during a given potential river flood event was linked with the scenarios used to generate
231 the flood hazard maps so that the appropriate maps were used to interpolate water depths. If the return period of the peak
232 discharge was below 10 years, water depths were extrapolated using two maps with the lowest return periods. No flooding was
233 assumed if the peak discharge was below the empirical 2-year return period derived from detrended 1950–2020 peak discharges
234 of the extracted flood events. This threshold was typically much lower than the 2-year return period derived with the
235 Generalized Pareto distribution. [Due to the logarithmic nature of the relationship between river discharge and water level, we](#)
236 [used the natural logarithm of discharge as basis of interpolation. The maps have different extents, therefore if an area is not](#)
237 [flooded in the map with a lower return period, the interpolation is between zero depth and water depth of the map with a higher](#)
238 [return period is made.](#)

239 Only grid cells with water depths of at least 10 cm were considered inundated, as in the maps of Dottori et al. (2022). The
240 individual flood maps for each river grid cell were aggregated within a NUTS3-level event. Finally, only those NUTS3-level
241 events were preserved for further analysis if the potential flood zone was at least 100 ha. At this point, the list of NUTS3-level
242 events was compared against the same list from the coastal model. If a river event in a given NUTS3 region occurred at the
243 same time as a coastal event in the same region, a separate “compound” event was created by merging the flood zones of the
244 coastal and riverine events in that region. The compound events are analysed in addition to the individual coastal and riverine

245 events, rather than replacing them. From here, processing of the potential flood events follows a common path for all types of
246 events.

247 **2.4 Combined flood catalogue**

248 **2.4.1 Aggregating and estimating potential losses per event**

249 Almost 250,000 potential flood events at the level of NUTS3 regions are aggregated for each country. One full calendar day
250 separates two country-level events consisting of at least one NUTS3 event. Coastal, riverine, and compound events are each
251 aggregated separately. Each event is characterised by hydrological parameters, such as inundated area, average water depth,
252 duration and return period. The latter is the geometric average of all river grid cells or coastal segments that contribute to the
253 flooded area.

254 Potential losses were estimated by multiplying exposure for each 100 m grid cell within each flood footprint with an appropriate
255 loss function. Exposure per grid cell (population and value of fixed assets) was computed with the HANZE v2.0 exposure
256 model (Paprotny and Mengel, 2023), which estimates historical exposure changes using a combination of rule-based and
257 statistical modelling that enabled downscaling past demographic and economic trends at subnational level into a high-
258 resolution grid. The model provides annual data for years 2000–2020 and 5-yearly timesteps for 1950–2000. Alongside
259 population, the model can generate values of tangible fixed asset stock in euros (constant 2020 prices and exchange rates) in
260 8 sectors (housing, consumer durables, agriculture, forestry, industry, mining, services, infrastructure).

261 Firstly, fatalities were estimated per each 100 m grid cell by multiplying the population with the death probability determined
262 by water depth. Due to the lack of velocity data or dike breach locations, only such a simplified approach can be used here.
263 We opted for the S-shaped depth-fatality function by Boyd et al. (2005) as presented in Jonkman et al. (2008), which shows
264 very low chance of death until water depths of approximately 3 m, i.e.:

$$265 \quad F_d = \frac{0.34}{1 + \exp(20.37 - 6.18d)} \quad (2)$$

266 where F_d is the mortality rate and d is the water depth in m.

267 The second indicator, people affected, is simply the total population within the flood footprint. Finally, economic losses were
268 estimated using a set of depth-damage functions for different economic sectors. We applied the logarithmic-type functions
269 proposed for Europe by Huizinga et al. (2017) that distinguish five sectors: agriculture, industry, commercial, infrastructure,
270 and residential. The functions were applied to the appropriate sector in the exposure model. It should be noted that whenever
271 “economic losses” are mentioned in this paper, they only refer to direct damage to tangible fixed assets, without considering
272 indirect impacts.

273 **2.4.2 Obtaining the final flood catalogue**

274 Estimated flood impacts of each event computed in the previous step were used to further filter the flood event catalogue only
 275 to those floods with significant potential for socioeconomic impacts. To qualify for the list, the event had to pass two thresholds
 276 simultaneously (Table 32):

- 277 ● Inundated area above a fixed threshold, and
- 278 ● At least one of two socioeconomic impact indicators (computed according to section 2.4.1):
 - 279 ○ people potentially affected above fixed threshold, or
 - 280 ○ potential economic losses above an event-specific threshold.

281 The exact threshold depends on the type of event, and in case of economic losses also on country and year of event, as it was
 282 linked to the level of gross domestic product (GDP) per capita (Table 32).
 283

284 **Table 32. Thresholds for selecting flood events with significant potential impacts and number of filtered events.**

Threshold	Coastal floods	Riverine and compound floods	<u>Compound floods</u>
<u>Threshold</u>			
Area inundated	1000 ha	2000 ha	
People affected	2500	5000	
Economic damage	10,000 times GDP per capita (country and year of event)	20,000 times GDP per capita (country and year of event)	
<u>Number of events by modelling step</u>			
<u>Regional-level aggregated events</u>	<u>22,446</u>	<u>213,517</u>	<u>5235</u>
<u>National-level aggregated events</u>	<u>4208</u>	<u>19,918</u>	<u>1452</u>
<u>Filtered events by impact thresholds</u>	<u>2436</u>	<u>11,205</u>	<u>1058</u>

285
 286 Thresholds in Table 32, as well as those described earlier in the methodology, were selected iteratively based on the following
 287 objectives:

- 288 ● Maximise the number of modelled events matching observed events from HANZE;
- 289 ● Maximise the share of one-to-one relationships between modelled and observed events (as opposed to many-to-one
 290 or one-to-many relationships);
- 291 ● Minimise the spatial extent of events in terms of affected NUTS3 regions beyond those indicated in HANZE;
- 292 ● Create a list of events large enough for statistical analyses and small enough to allow manual searches of historical
 293 records for all events.

294 To help select the thresholds, observed flood events from the following six datasets were matched per country according to
 295 start and end dates:

- 296 • HANZE v2.1 (Paprotny et al., 2023);
- 297 • EM-DAT (Centre for Research on the Epidemiology of Disasters 2023);
- 298 • EEA Flood Phenomena (from 1980 only) (European Environment Agency, 2015);
- 299 • Dartmouth Flood Observatory (from 1985 only) (Brakenridge, 2023);
- 300 • FFEM-DB (from 1980 only) (Papagiannaki et al., 2022);
- 301 • Recorded Flood Outlines (England only) (Environment Agency, 2023).

302 In addition, the HANZE dataset was matched with events below the tested thresholds-. Following the above objectives results
 303 in different potential impact thresholds for coastal and riverine floods. [In total, some 43% of events were filtered out \(Table](#)
 304 [2\).](#)

305 2.4.3 Comparing modelled and reported events

306 The modelled flood events of the catalogue were evaluated using gauge records and impact data as well as manual research
 307 involving all kinds of documentary sources. At first, English-language papers and local-language flood catalogues providing
 308 an overview of the hazard in the country were consulted. Then, national disaster databases were searched and the relevant data
 309 was extracted. Papers on case studies of disasters were searched for in both English and the local language of the country being
 310 researched. A keyword-based search in both English and the local language was performed using a web engine to identify
 311 news articles or other online reports mentioning the relevant disasters. In total, 946 major text or data sources were used, 828
 312 of which are listed in the HANZE v2.1 dataset (Paprotny et al., 2023) and the remainder is listed together with the data from
 313 this study. Based on this information on impacts, each event was categorised into one of the classes listed in Table [43](#).

315 **Table 43. Classification of flood events considering the availability of data sources as well as reported hydrological and socioeconomic**
 316 **impacts. [All classes are included in the final flood catalogue.](#)**

Class	Short name	Evaluation result	
		Extreme hydrological event	Inundation with significant socioeconomic impacts
A	Impacts, data	Confirmed by sources	Confirmed by sources (impact data available)
B	Impacts, no data	Confirmed by sources	Confirmed by sources (impact data not available)
C	No impacts	Confirmed by sources	Not confirmed by sources
D	Unknown impacts	Confirmed by sources	No sources available
E	False positive	Not confirmed by sources	Not confirmed by sources or no sources available
F	No information	No sources available	No sources available

317
 318 In applying the classification from Table [43](#), a decision graph from Fig. [1+2](#) was used. In general, in case of complete lack of
 319 gauge data or documentary sources, the event was labelled F (“No information”), meaning that no observational data is
 320 available and therefore modelled data can be neither confirmed or rejected. In case gauge records are available, it was firstly
 321 evaluated if they indicate extreme values. Exceedance of a 2-year return period was considered sufficient to confirm that the

322 modelled event was an extreme hydrological event in real life. If the threshold was not exceeded at any of the available gauge
323 stations, the time series was analysed, and the event was considered confirmed as hydrologically extreme if a flood wave was
324 clearly visible at the dates indicated by the model. If no flood wave was visible, the event was considered a “False positive”
325 (label E), i.e. an error of the model that indicates a too high simulated river discharge or sea level. In rare cases, this
326 classification was overridden if documentary sources indicated the occurrence of a flood event. It should be noted that “false
327 positives”, like all other classes, are maintained in the final flood catalogue, so that the users of the data could decide whether
328 include them in their analyses or not.

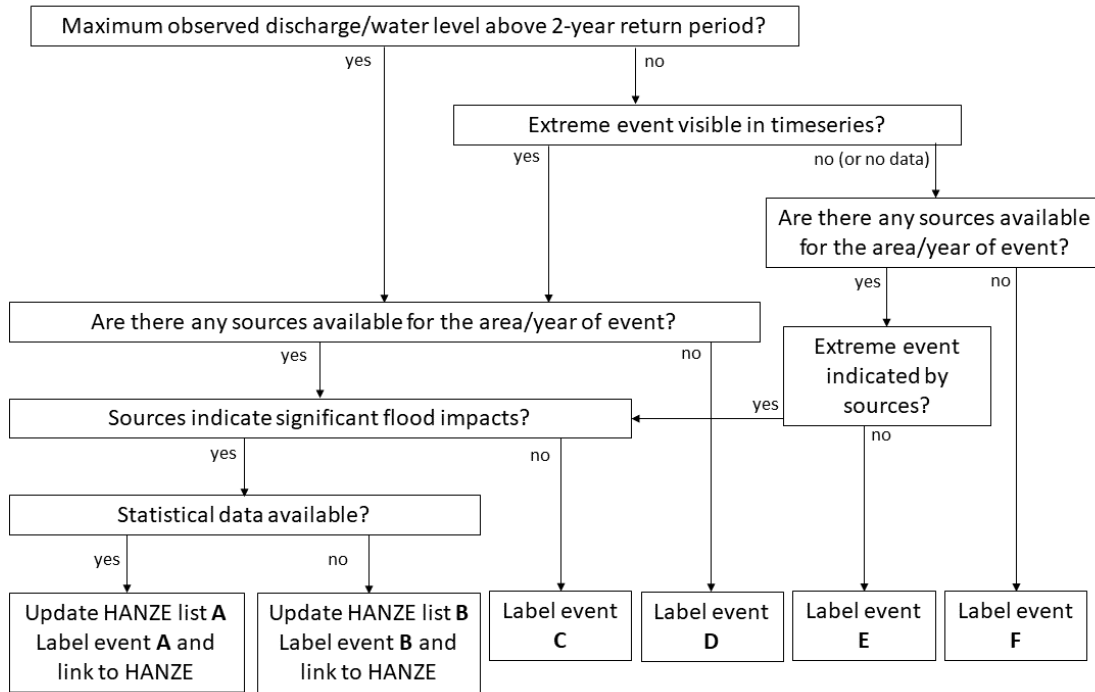
329
330 For events confirmed as hydrologically extreme, further analysis concentrated on the occurrence of significant socioeconomic
331 impacts. Here, significant impacts were defined as in the HANZE database (Paprotny et al., 2023), i.e. exceedance of at least
332 one the following thresholds:

- 333 ● At least 1000 ha (10 km²) inundated;
- 334 ● At least one person killed or missing presumed dead;
- 335 ● At least 50 households or 200 people affected, defined preferably as affected by their homes being inundated by
336 floodwaters, or who were evacuated from the inundated area, if the preferred statistic was not available;
- 337 ● Losses in monetary terms corresponding to at least 1 million euro in 2020 prices.

338 In case no further information was available, the event was labelled D (“Unknown impacts”). If despite good coverage of
339 sources (e.g. comprehensive local/national flood databases or catalogues), no impacts are mentioned, or in rare cases, direct
340 statement that e.g. a flood emergency did not result in breaching of flood defences, the event was labelled C (“No impacts”).
341 Also, if data on impacts were available, but they did not pass any of the aforementioned thresholds, the event was labelled as
342 “No impacts”. Events with sufficient information on significant impacts were labelled A (“Impact, data”) and incorporated
343 into the HANZE database. However, if statistical data was not accessible, or referred only to a small part of the impacted area,
344 but available descriptions strongly indicated that one of the impact thresholds was likely exceeded, the event was recorded in
345 a separate list of events, labelled B (“Impact, no data”). Available historical information was collected for such an event in a
346 database that is a simplified version of HANZE. Detailed description of the data collected in this database, which is made
347 publicly available with this study, is provided in Appendix A1. It should be noted that a matching of dates and country with
348 historical events was not enough to label the event A or B. For that, at least one NUTS3 region affected during the event had
349 to be correctly identified by the model.

350 Additional provisions were made for compound events. If a potential ‘compound’ flood is indicated in the catalogue, but based
351 on reports and observations impacts can be attributed only to a coastal flood, the compound event was labelled C (“No
352 impacts”), the corresponding coastal event as A or B, and the corresponding riverine event as C. The same approach was used
353 if only the riverine driver was responsible for impacts. Also, if a single-driver event was found to be a “false positive” (label
354 E), the corresponding compound event was also classified as “false positive”. In this way, the compound flood definition for

355 [events labelled A and B is consistent with the HANZE database, where the interaction of coastal and riverine components is](#)
356 [required for a flood to be classified as compound.](#)
357



358
359 **Figure 21. Decision graph for classifying flood events.**
360

361 The final flood catalogue consists of two components: (1) a table with all events, indicating their timing, location, potential
362 impacts, hydrological parameters and classification, and (2) potential flood footprint maps in vector format. The data contained
363 in the table are explained in Appendix A2.

364 2.5 Validation

365 Validation of river discharges is presented by Tilloy et al. (2024), however we used the 3442 stations containing daily
366 observations collected for that study for further analysis. The dataset helped us to classify the events in section 2.4.3. Further,
367 we compared extreme discharges observed during riverine and compound events with modelled discharges. Station data was
368 obtained in 60% from the Global Runoff Data Centre and in 40% from national public datasets of France, Norway, Poland,
369 Spain, Sweden and the United Kingdom. The analysis was limited to 2914 stations with an upstream area of at least 100 km²,
370 located in the affected NUTS3 regions according to the model. If the event duration and available gauge series were both at
371 least 30 days, the daily discharge was compared using the Kling–Gupta efficiency, or KGE (Gupta et al., 2009), and

372 Spearman’s coefficient of determination (as Pearson’s is used in the KGE score). Otherwise, an equal amount of days was
373 added before and after the event, so that at least 30 observations are used. The maximum daily discharges during the event
374 were also compared.

375 Validation of the hourly storm surge heights, tide elevations and combined water level was done using 428 tide gauges. Almost
376 all stations (413) were gathered from GESLA v3 dataset (Haigh et al., 2023), but for better coverage of the eastern
377 Mediterranean Sea it was complemented with 7 stations from Poseidon System (2023), and for the southern Baltic Sea with 8
378 stations from the Institute of Meteorology and Water Management – National Research Institute (2023). Apart from validation
379 for all available time series, an event-based validation was done as for river discharges. The default time window for the
380 comparison between modelled and observed data was 7 days, unless the event had a longer duration.

381 Finally, the modelled flood footprints were compared with satellite-derived footprints from the Global Flood Database (GFD,
382 Tellman et al., 2021). The footprints were converted into vector layers, with permanent water bodies removed from them, as
383 per data contained in GFD. Only footprints within NUTS3 regions indicated as affected in the HANZE database were included
384 in the analysis. Population affected within the footprints was derived from HANZE population maps. Flooded area and
385 population affected based on footprints from this study and GFD were compared with reported impacts. Additionally, all flood
386 events in the catalogue with comparative reported impact data were analysed for the difference in modelled and reported
387 impacts. Ideally, all modelled impacts should be higher than what was reported, as the intention of the catalogue is to generate
388 potential footprints that do not consider flood protection. Finally, footprints from this study and GFD were intersected to derive
389 the hit rate, i.e. share of the satellite footprints correctly reproduced by the model. This is a similar approach that was used to
390 validate flood hazard maps that are the basis of the modelled footprints (Vousdoukas et al., 2016b, Paprotny et al., 2017,
391 Dottori et al., 2022).

392 **3 Results**

393 **3.1 Flood event catalogue**

394 **3.1.1 Modelled impacts by classification**

395 The final catalogue includes 2436 coastal, 11,205 riverine, and 1058 compound events with significant potential for
396 socioeconomic impacts (Fig. 23). This already indicates a significant proportion of coastal and riverine events might be
397 compound events. The spatial location and timeframe of events was matched with at least some gauge observations for 63%
398 of coastal and 72% of riverine events. By applying the 2-year return period threshold to observational data, it was possible to
399 immediately confirm that 40% of coastal and 45% of riverine events were hydrologically extreme. Further confirmations were
400 obtained through analysis of gauge timeseries and documentary records, increasing the confirmation rate to 80% for coastal,
401 77% for riverine, and 66% for compound events. On the other hand, no extreme event was indicated by gauge or documentary

sources for a small part of the catalogue. The false positive ratio (“E” events to “A”-“D” events) amounts to only 2.2% (16) for compound, 3.3% (67) for coastal, and 5.2% (474) for riverine floods.

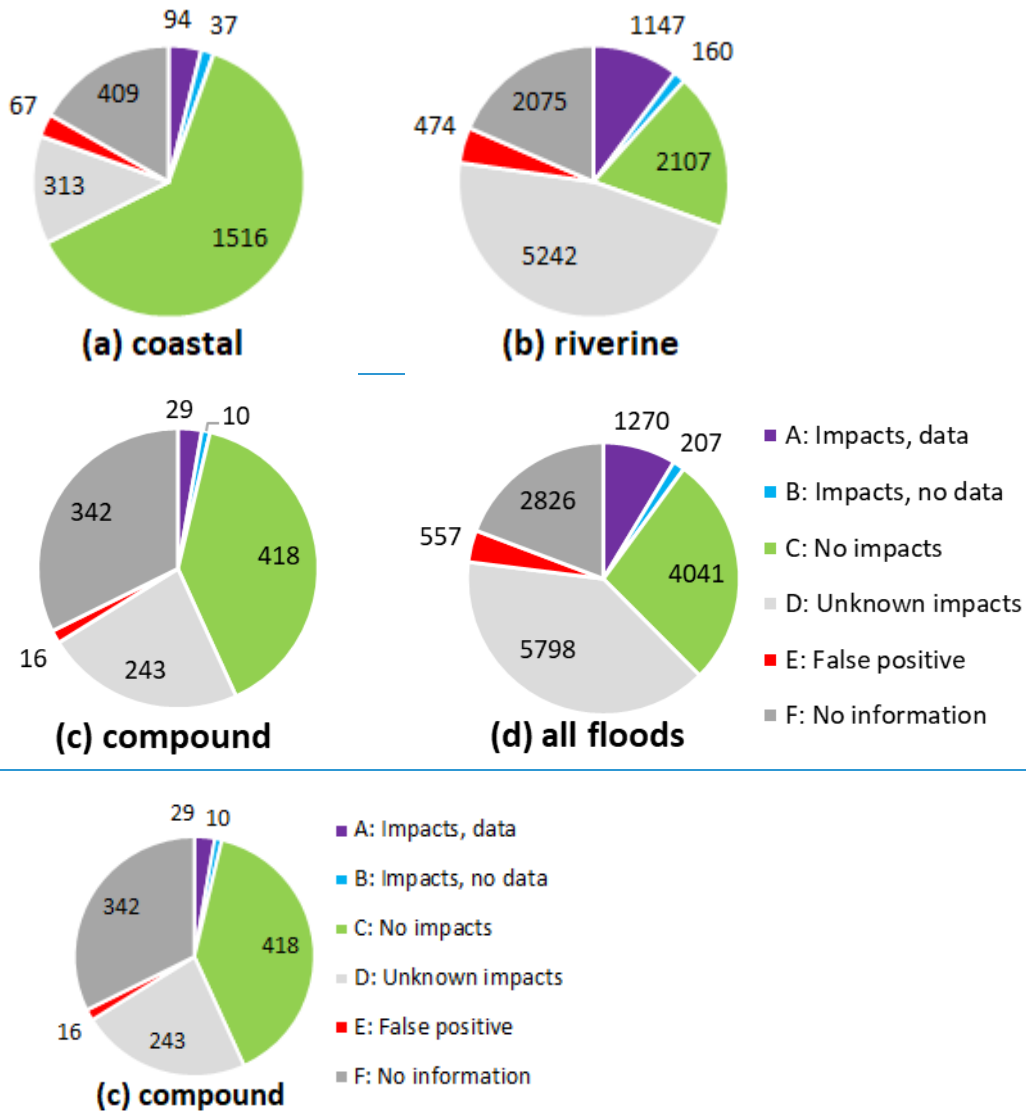
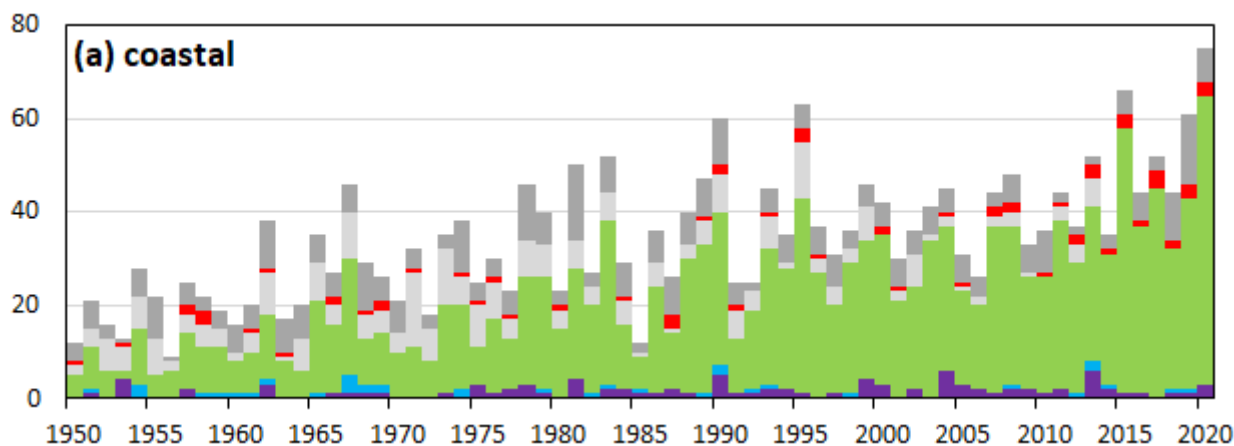


Figure 23. Flood events in the catalogue by classification: (a) coastal, (b) riverine, and (c) compound. Panel (d) shows totals for all events.

Confirmation, or at least high confidence based on available documentary sources, whether the event did, or did not, result in significant socioeconomic impacts was possible for the majority of coastal and compound events, but not for riverine floods. However, the latter occurred by far most frequently, and it was possible to confirm significant socioeconomic impacts for

414 11.7% of riverine (1307), 5.4% of coastal (131), and 3.7% of compound (39) events (Fig. 23). In some cases, “A” (“Impacts,
415 data”) events correspond to more than one reported flood in the HANZE database, or the events are a combination of “A” and
416 “B” (“Impacts, no data”)-type events. Therefore, the 1270 “A” and 207 “B” events actually correspond to 1471 historical
417 floods in HANZE and 237 historical floods without impact data collected in a separate dataset as part of this study (see
418 Appendix A1). This statistic excludes a small number of events that were below the significant impact threshold, but indicated
419 a temporal match with the HANZE database. Only 109 such events were identified, of which only two were coastal events and
420 two were compound events. Out of those, only 33 events, all riverine, were spatially matched with HANZE, a single historical
421 flood in each case. This constitutes only 2% of matched HANZE events, hence we can deem the hydrological and
422 socioeconomic thresholds in this study as well designed, as few HANZE events were missed due to their imposition without
423 creating too many non-impact events. Also, while there were many one-to-many matches between our model and HANZE,
424 largely due to the data-availability rules causing splitting of some flood events in HANZE, there were only a handful of cases
425 of many-to-one connections.

426 The distribution of events over time (Fig. 34) shows an upward trend, which in case of “A” and “B” events is largely related
427 to better availability of data. There is also better confidence in non-occurrence of impacts for coastal and compound events in
428 recent decades compared to the beginning of the timeseries. An increase in “F” events in the final few years for riverine and
429 compound events is primarily connected with lower availability of recent river gauge data.
430



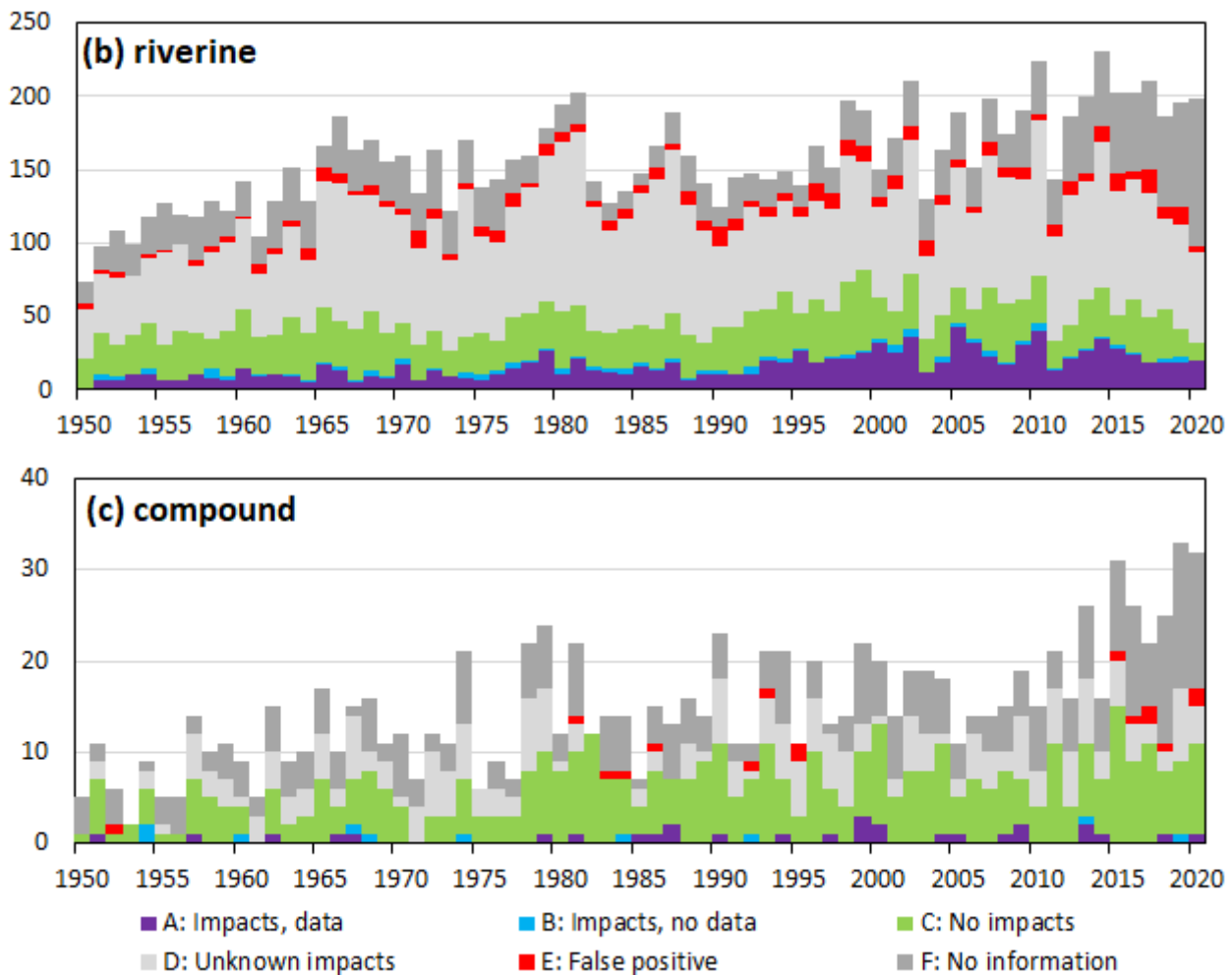
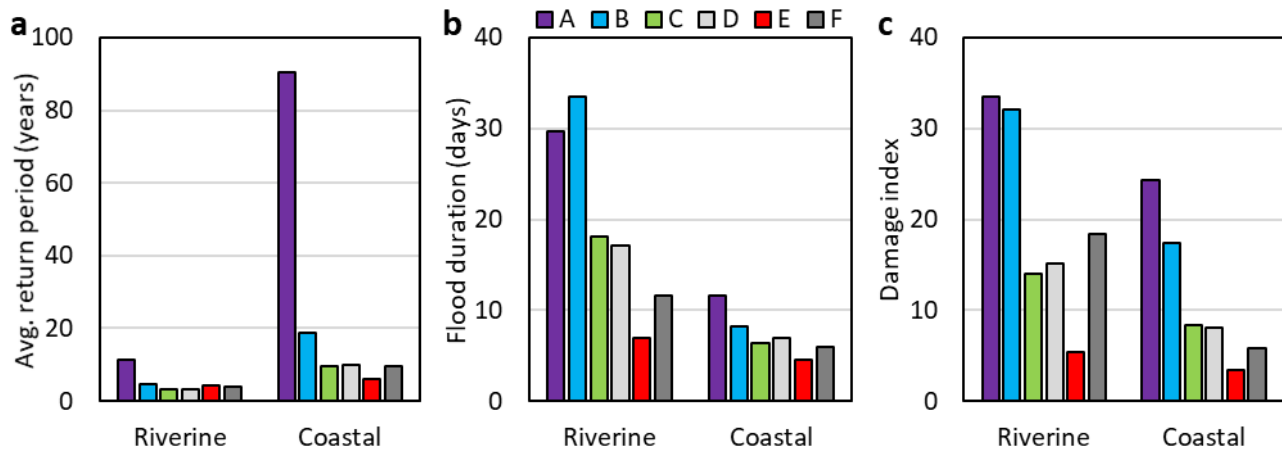


Figure 34. Flood events in the catalogue by year and classification: (a) coastal, (b) riverine, and (c) compound.

Modelled extremity and impacts of events vary strongly by class (Fig. 45). The return period along affected river and coastal segments is generally much higher for “A” and “B” events compared to all others. 18% of coastal and 37% of riverine events, in which the geometric average of return periods in the affected area was above 25 years, was classified as either “A” or “B”. In contrast, when the return period was below 5 years, the values were 2% and 10%, respectively. Interestingly, the occurrence of “F” class (“No information”) was only slightly lower for higher return periods. Confirmed impactful events were also longer in duration than other classes, with false positives (“E”) having the shortest duration. Consequently, the “A” and “B” events had, on average, the highest impact potential. In Fig. 4e5c, the dimensionless damage index is the average of four impact categories (potential area inundated, fatalities, persons affected, and economic loss) relative to maximum impact of any event in the country during 1950–2020 at constant 1950 exposure. False positives had, on average, the lowest impact potential. In

445 all examples, the remaining categories (“C” – No impacts, “D” – Unknown impacts, and “F”) oscillated around the average
 446 values for all variables analysed in Fig. 45.
 447



448
 449 **Figure 45.** Comparison of mean values of selected indicators by main flood type and classification: (a) average return period along
 450 affected river or coastal segments, (b) total flood event duration, (c) dimensionless damage index, where 100 equals the highest
 451 potential impact of any event in the country during 1950–2020 at constant exposure.

452 3.1.2 Comparison with HANZE reported impacts database

453 The flood catalogue includes the majority of reported historical floods with significant socioeconomic impacts since 1950
 454 contained in the HANZE v2.1 database (Paprotny et al., 2023). However, there is a strong difference between the completeness
 455 of the catalogue according to flood type. While about 90% of coastal, compound and slow-onset riverine floods were modelled,
 456 only 55% of flash floods were captured (Table 54). The latter category, as defined in HANZE, represents short, rapid floods,
 457 where the extreme rainfall event triggering the event lasted no more than 24 hours, excluding urban floods. As those often
 458 occur in small catchments, they are often not captured as the study was limited only to catchments with an upstream area of at
 459 least 100 km².

460 The HANZE database indicates more than 6,000 NUTS3-level impacts since 1950. 78% of those are reproduced by the model
 461 (Table 54), a slightly higher percentage than the hit rate at event level (74%). This is largely due to good coverage for slow-
 462 onset riverine floods (88%) compared to flash floods (55%), when the former affected more regions on average than the latter.
 463 For the 1504 events matched by the model, the hit rate of NUTS3 regions for the model is 89%, again lower for flash floods
 464 (84%) than for larger riverine events (91%), not to mention coastal floods (98%). A full list of HANZE events with the
 465 information which of those were captured by the model, and which NUTS3 regions were correctly identified is provided
 466 together with the dataset on the repository (Paprotny, 2024). In general, performance of the model is stable over time (Fig. 56),
 467 though the share of events correctly identified by the model is lower in the very beginning of the model runs (1950s).

468 Analysing the reported impacts in HANZE, even though they are incomplete (except for fatalities), provides further insights.
469 The data in Table 5-4 show that 97–100% of reported impacts in all four categories for coastal, compound and slow-onset
470 riverine floods were in those historical floods that could also be found in the model. This shows that the model captured almost
471 all large events, and the omissions are mostly minor floods in specific areas where the hazard is apparently not well quantified.
472 For instance, out of 14 omitted coastal and compound floods, 10 are events in Italy occurring mostly before 1964 and affecting
473 200–500 persons with no more than one fatality (with a single exception of a seven-fatality flood from January 1950). Much
474 lower coverage is again for flash floods, as only those responsible for 61% of all fatalities can be found in the model. For other
475 impact categories, the coverage is better, but historical records are very incomplete in relation to those statistics.

476

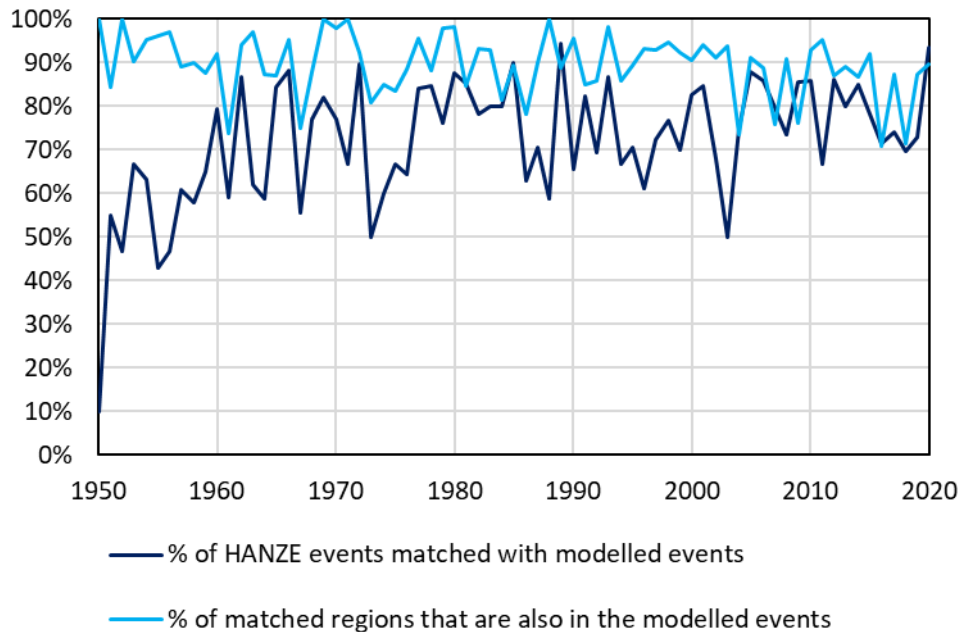
477

478
479
480

Table 5.4. Comparison of the number of HANZE events, their footprints and reported impacts, with modelled data, 1950–2020. * only regions classified as compound by the model – regions forming compound events in the HANZE database are not necessarily in the zone directly influenced by both riverine and coastal drivers; ** impact data is not available for all HANZE events.

Category	HANZE event type				All events
	Coastal	River/ Coastal	River	Flash	
<i>Matching of events with impact data (“A” events)</i>					
Number of events in HANZE database (1950–2020)	71	41	970	955	2037
Number of modelled events matched with HANZE	61	37	880	526	1504
Percentage of HANZE events matched with modelled events	90%	86%	91%	55%	74%
<i>Matching of affected NUTS3 regions</i>					
Number of affected NUTS3 regions in HANZE database	195	162	4058	1671	6086
Number of affected NUTS3 regions in matched HANZE events	180	152	3910	1084	5326
Number of regions that are also in the modelled events	177	97*	3553	915	4742
Percentage of all regions that are also in the modelled events	91%	60%*	88%	55%	78%
Percentage of matched regions that are also in the modelled events	98%	64%*	91%	84%	89%
<i>Percentage of total reported impacts of all HANZE events within matched HANZE events (1950–2020) **</i>					
Area inundated	99.8%	100%	99.5%	93.2%	99.2%
Fatalities	99.5%	99.4%	97.0%	61.2%	81.2%
Persons affected	99.3%	98.7%	98.9%	78.9%	96.3%
Economic losses in 2020 euros	99.8%	100%	98.9%	86.1%	96.1%
<i>Matching of events without impact data (“B”)</i>					
Number of historical floods without impact data (list B)	27	12	119	79	237

481



482
483 **Figure 56.** Share of HANZE events matched with the model, and the share of regions in matched events also present in the model.
484

485 3.2 Modelled potential impacts in the flood catalogue

486 Without flood protection measures, floods would have large consequences throughout Europe. A simple summation of flood
487 impacts in the catalogue is not informative, as it assumes not only no flood protection, but also that population and economic
488 activity move into the frequently affected zone in the first place, and then immediately return to previous conditions after each
489 event, even just days after the previous. Considering the total reported impacts in HANZE v2.1, albeit incomplete, it can be
490 estimated that only about 1% of potentially inundated area, population and economic assets were actually affected during
491 1950–2020. The reported flood deaths equal only about 0.01% of the potential fatalities. Therefore, the potential impacts are
492 merely an intermediate result necessary in the process of estimating flood vulnerability and impact attribution (see section 5).
493 Still, some analysis of the results can be performed as the modelling chain can derive the impact estimates under different
494 exposure scenarios, and it was driven by variable climate conditions.

495 3.2.1 Temporal changes in potential flood impacts

496 For all types of events, an increase in the number of potential events and their impacts was recorded (Table 65). Even though
497 the trends are less pronounced under constant exposure scenarios, they are still equivalent to at least 0.3% annual 21% increase
498 in potential coastal flood losses in an average year between 1950 and 2020 in case of fatalities, 470.5% in case of economic
499 loss and 0.875% in case of affected population. For riverine floods, the potential impacts have grown even more, while the

500 strongest increase is indicated for compound floods, at ~~least threefold since 1950~~ [a rate of at least 1.9% per year since 1950](#).
501 Potential impacts per flood event are rather similar for coastal and riverine events, and slightly lower for compound events, as
502 the latter category is spatially constrained to regions directly affected by both coastal and riverine drivers.
503 Demographic and economic growth since 1950 has increased potential losses substantially. Presently, exposure of population
504 to riverine floods is more than 50% higher than if population would have not increased, and nearly twice as high for coastal
505 and compound events. Potential impacts relative to the total population in the study area increase more strongly than in the
506 constant-exposure scenario, indicating stronger population growth in areas prone to coastal and compound flooding relative to
507 areas not at risk. However, only a marginal increase in areas at risk of riverine floods was observed relative to areas not prone
508 to this type of floods.
509 Enormous increase in gross domestic product (GDP) per capita (2% per year in the study area), and associated growth in the
510 stock of fixed assets resulted in a five- to six-fold increase in potential losses relative to 1950, and eight- to ten-fold increase
511 in 2020. As the asset growth was higher than GDP, potential economic losses relative to GDP also increased between 1950
512 and 2020. In contrast to population growth, asset growth in flood-prone areas was only marginally higher, or even lower in
513 case of riverine events, than in areas not at risk of flooding.
514
515

516
517
518

Table 65. Average potential impacts of floods and their trends, by flood type and exposure scenario (dynamic year-of-event exposure, or fixed at 1950 or 2020 levels). The impacts of compound events mostly overlap with those of coastal and riverine, therefore they should not be added together. Economic losses in constant 2020 prices and exchange rates.

Flood type	Coastal			Riverine			Compound		
Exposure map	Dyna- mic	1950	2020	Dyna- mic	1950	2020	Dyna- mic	1950	2020
<i>Average potential impacts per year</i>									
Number of events	34	x	x	158	x	x	15	x	x
Area inundated (thsds. km ²)	27	x	x	182	x	x	13	x	x
Fatalities (thousands)	214	133	351	1,059	851	1,246	81	51	108
Persons affected (thousands)	2,689	1,966	3,590	15,284	11,919	18,247	1,004	704	1,239
Economic loss (billion euro)	237	50	478	1,200	261	2,196	86	14	149
<i>Annual increase of potential impacts (%)</i>									
Number of events	1.3	x	x	0.7	x	x	1.5	x	x
Area inundated	1.1	x	x	0.4	x	x	1.6	x	x
Fatalities	1.5	0.4	0.3	1.0	0.6	0.6	2.6	1.6	1.9
Persons affected	1.5	0.9	0.8	1.2	0.8	0.8	2.4	1.7	1.9
Economic loss	2.8	0.6	0.5	3.1	0.9	0.9	4.0	1.8	2.0
<i>Increase in total impacts relative to 1950 exposure</i>									
Fatalities	61%	x	164%	24%	x	46%	59%	x	111%
Persons affected	37%	x	83%	28%	x	53%	43%	x	76%
Economic loss	371%	x	852%	360%	x	742%	505%	x	948%

519

520 3.2.2 Spatial distribution of potential flood impacts

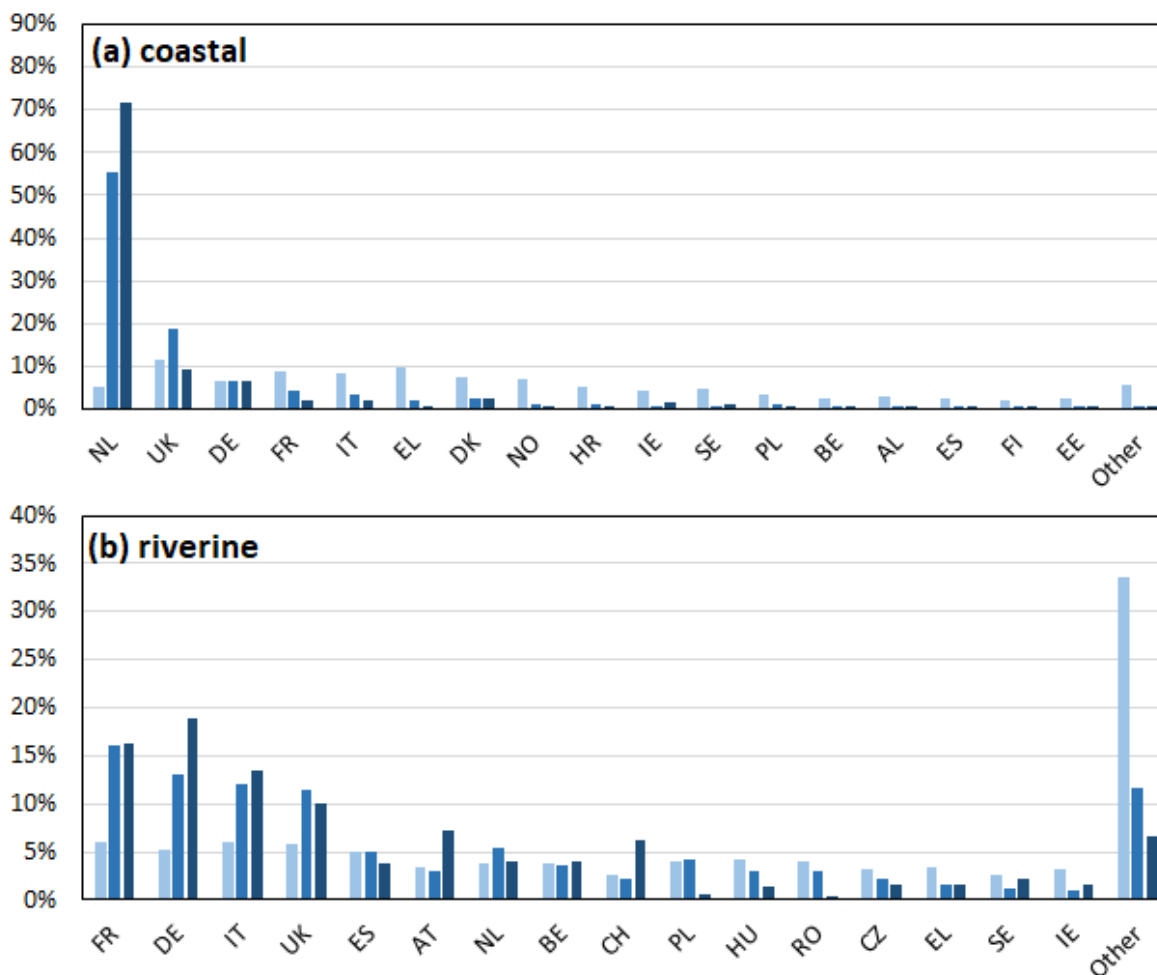
521 Coastal and compound flood potential is highly concentrated in just a few countries (Fig. 67). Though these estimates do not
522 include the effect of flood protection, the top five countries by coastal flood potential are also most prominently featured in
523 the HANZE database in terms of historical coastal flood impacts: the Netherlands, the United Kingdom, Germany, France,
524 and Italy. The same group, plus Ireland, also have the most significant compound flood potential. On the other hand, numerous
525 potential coastal and compound floods are present in the catalogue for Greece, but only one historical example for that country
526 could be found in HANZE (a compound flood in 1968 that affected Crete).

527 In total, the flood catalogue includes coastal floods in 25 countries and compound floods in 24. Slovenia also has no event on
528 the compound flood list, as none of the compound events was able to pass the higher socioeconomic thresholds for riverine

529 and compound events. Bosnia and Herzegovina and Montenegro are the only countries on the compound flood list that are not
 530 present on the coastal flood list due to the limited risk along their short coastlines. Bulgaria is the only country with access to
 531 the sea that is not included in the coastal flood catalogue, as no event exceeded the socioeconomic thresholds. One historical
 532 case of coastal flooding in Bulgaria (in 1999) was recorded in HANZE.

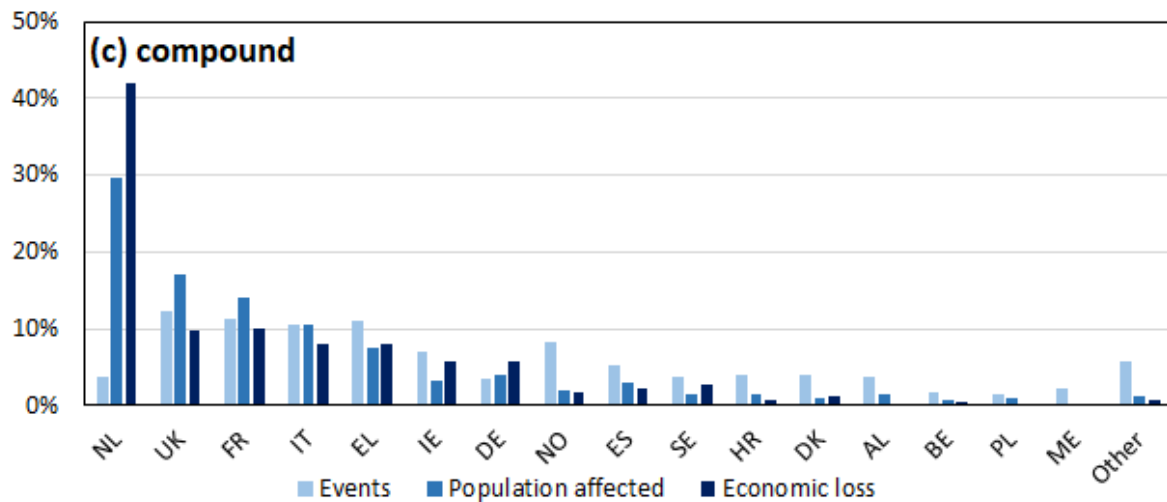
533 Riverine flood potential is more evenly distributed in space. All countries highlighted in Fig. 6b-7b have numerous examples
 534 of historical damaging floods in HANZE, with the exception of the Netherlands, where historical cases are limited to four
 535 floods recorded in the 1990s. In total, 37 out of 42 countries in the study area had at least some potential flood events. Some
 536 small countries had no riverine or compound floods in the catalogue, as they have no river section with an upstream area bigger
 537 than 100 km².

538



539

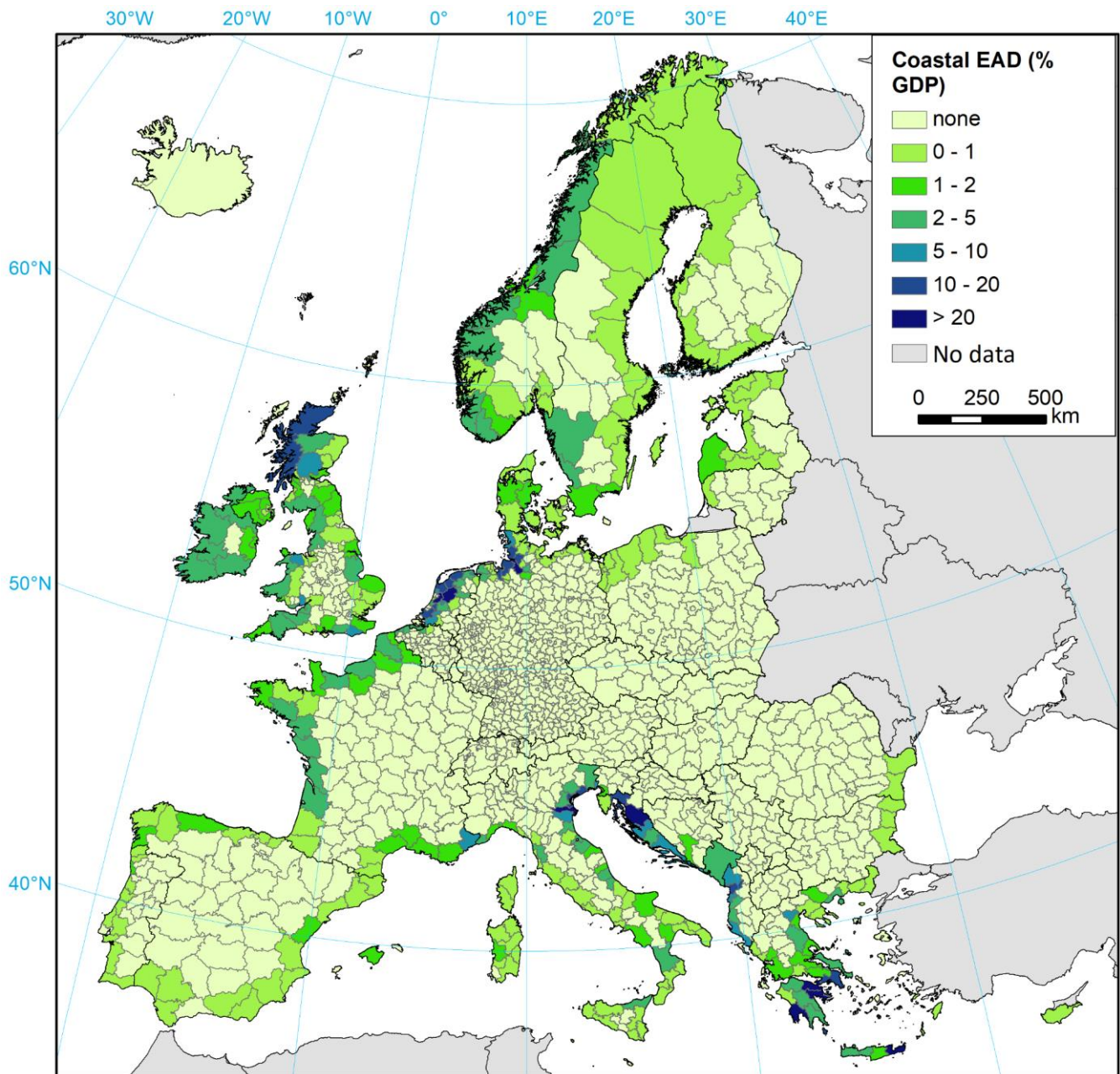
540



541
542 **Figure 67.** Flood events in the catalogue by country and potential impacts, as % of all events: (a) coastal, (b) riverine, and (c)
543 compound. Population affected and economic loss in constant 2020 exposure.

544
545 A variety of indicators can be derived at the level of NUTS3 regions. Here we present one example, potential economic
546 damages normalised to 2020 exposure level, relative to 2020 gross domestic product (GDP). Along most of the European coast
547 potential damages resulting from storm surges are limited (Fig. 78), with risk concentrated along the North Sea, Adriatic Sea,
548 and Aegean Sea. Locations of the most significant past coastal floods stand out (the Netherlands, German Bight, Venice).
549 Riverine damage potential is much higher (Fig. 89), and concentrated around main European mountain ranges (Alps,
550 Carpathians, Pyrenees, Dinaric Alps), as well as Scandinavia and British Isles. Risk is noticeably lower along the Northern
551 European Plain, southwestern Iberian Peninsula, and southern Great Britain. However, it must be stressed that the data
552 represent only damage potential, without considering flood protection or other forms of adaptation.

553 In some parts of Europe, the possibility of co-occurrence of coastal and riverine floods could have large implications on risk.
554 Fig. 9-10 maps the share of compound flood potential at regional level relative to the total. For each NUTS3 region, we derived
555 a list of all flood events with a potential inundated area of 100 ha, i.e. before aggregation and application of socioeconomic
556 thresholds, then removed riverine and coastal events that overlapped with compound events. In this way, it was possible to
557 avoid double counting and sum together the remaining flood events. The results (Fig. 9-10) show that compound potential is
558 very unevenly distributed across Europe. In northern and eastern coasts of the Adriatic Sea, Greece, Ireland, western and
559 southern coasts of Great Britain, and certain parts of France, Italy, Spain, and Norway, compound events could potentially
560 contribute 20–25% or even more of all economic losses from flooding. In all aforementioned countries there are known
561 examples of damaging floods contained in the HANZE database.



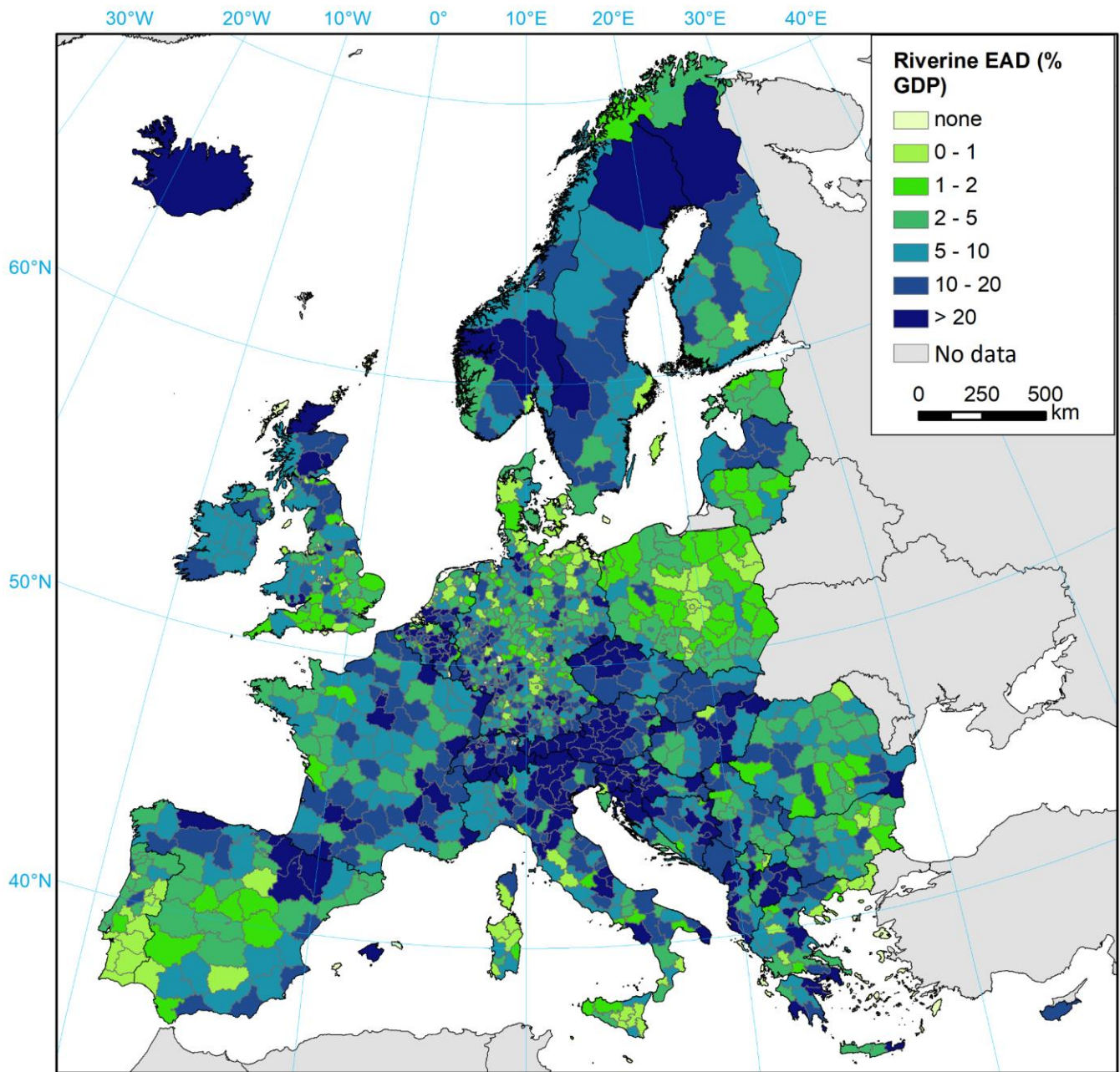
563

564

Figure 78. Potential expected annual economic damage of coastal floods as % of GDP, 1950–2020, in constant 2020 exposure, per NUTS3 region. Potential impacts per region include all events above 100 ha flooded area threshold per NUTS3 region, including those not passing the socioeconomic impact thresholds.

565

566



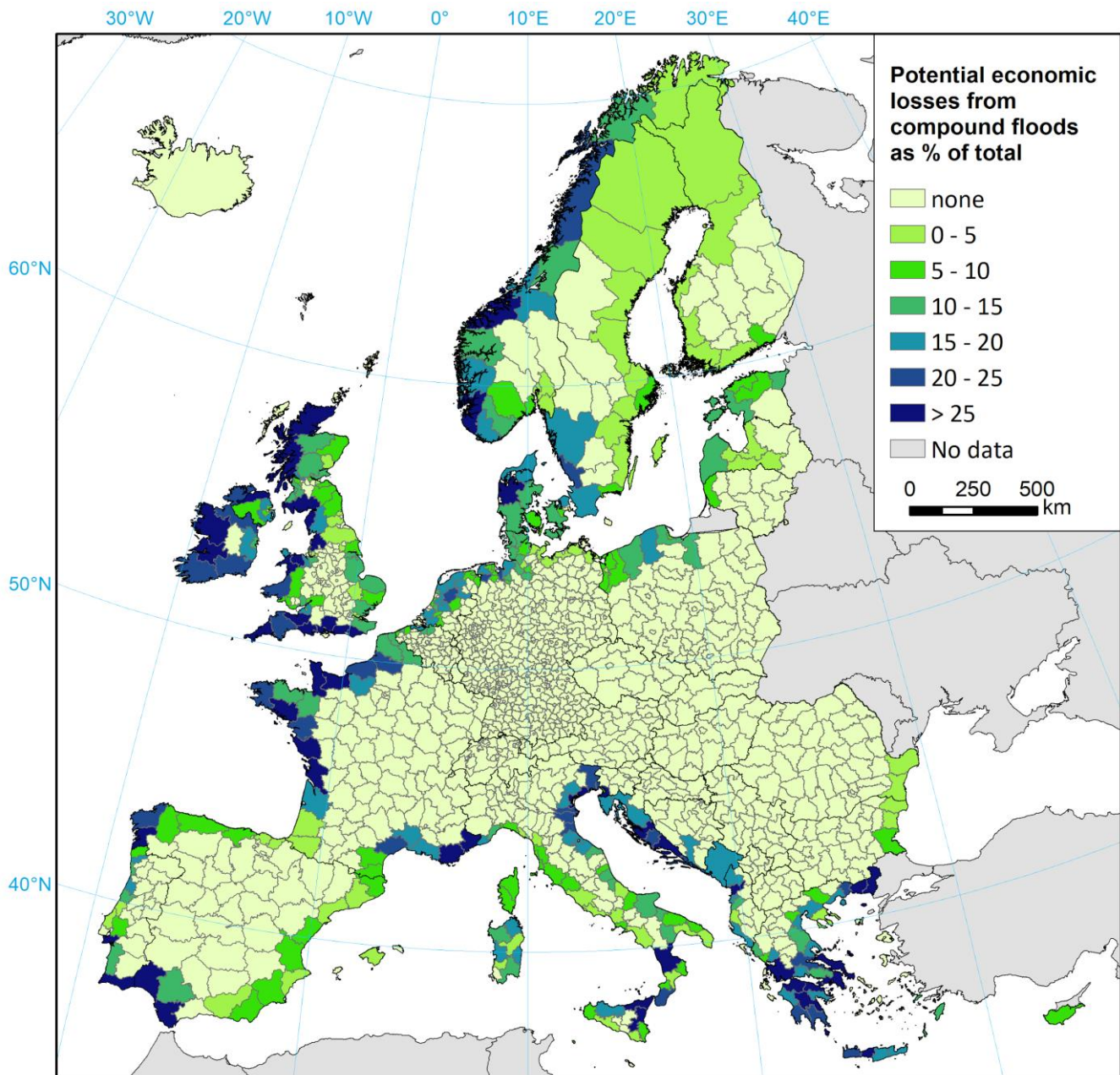
567

568

569

570

Figure 89. Potential expected annual economic damage of riverine floods as % of GDP, 1950–2020, in constant 2020 exposure, per NUTS3 region. Potential impacts per region include all events above 100 ha flooded area threshold per NUTS3 region, including those not passing the socioeconomic impact thresholds.



571

572 **Figure 910.** Share of compound floods is total potential economic losses, 1950–2020, in constant 2020 exposure, per NUTS3 region.
 573 Potential impacts per region include all events above 100 ha flooded area threshold per NUTS3 region, including those not passing
 574 the socioeconomic impact thresholds. Individual riverine and coastal events contributing to compound events were excluded to
 575 compute this metric.

576 **3.3 Validation**

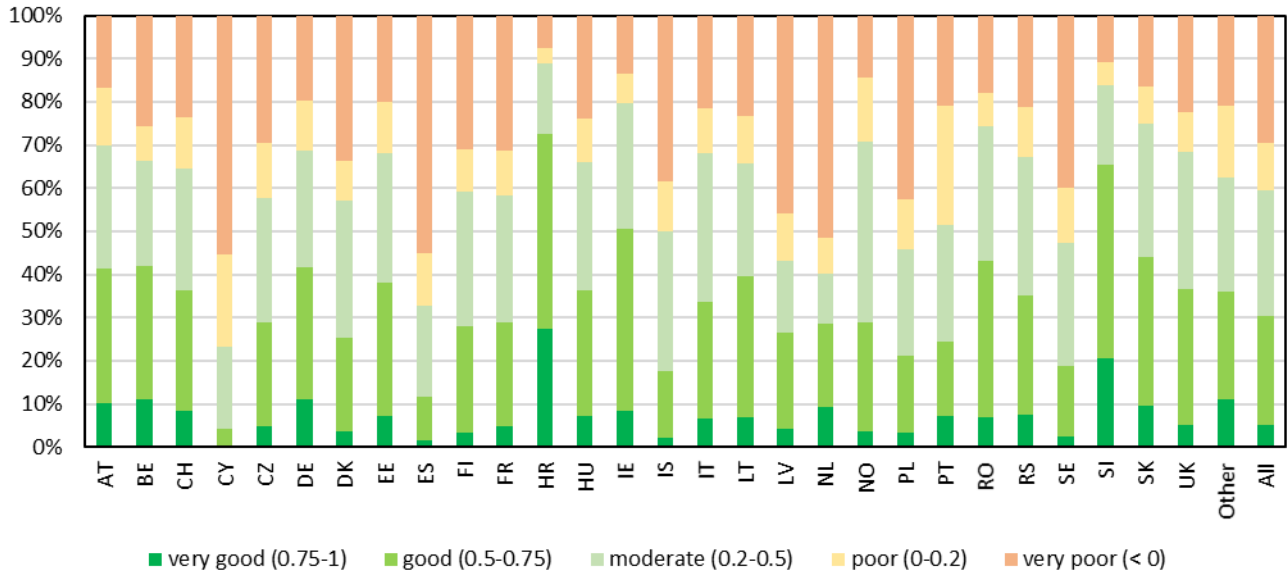
577 **3.3.1 Extreme river discharges**

578 At least one river discharge station with adequate data length was available for 7742 events (63% of the total), and nearly
579 292,000 timeseries were identified within the NUTS3 regions potentially affected by those events. Most of the data is available
580 for events that have occurred in the United Kingdom, Poland, Spain, Sweden, Germany, France, and Norway. The R^2 between
581 modelled and observed peak discharge for all event time series, standardised by reported upstream area, is 0.45. However, the
582 relative discharges are more of interest of this study, and modelled peak discharges corrected for difference in average annual
583 discharges have an R^2 of 0.63. The timeseries of daily discharge during the events is good (0.5-0.75) or very good (0.75-1) for
584 59% of all station-events in terms of Spearman's R^2 , and for 30% in terms of KGE score. On the other hand, poor (0-0.2) or
585 very poor (<0) performance was recorded for 18% and 41% of stations, respectively. There is relatively little difference in
586 performance depending on classification of events, except for far worse results for events classified as false positives ("E").
587 Here, the poor or very poor score was recorded for 83% of station-events, compared to 37% for HANZE flood events ("A").
588 Performance also varies strongly by location (Fig. [1011](#)), with e.g. Germany, Ireland, Austria, Belgium, and Slovakia recording
589 much higher shares of good or very good station performance (above 40%) than e.g. Poland, Spain, Sweden, and Portugal (less
590 than 25%).

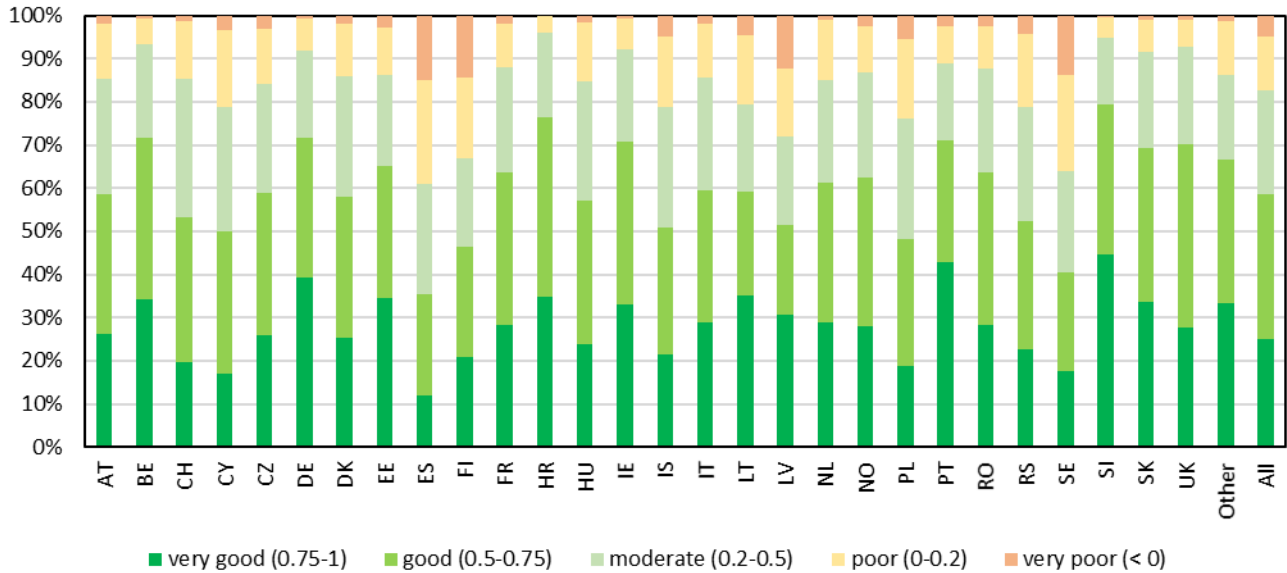
591

592

a



b



595

596

597

Figure 1011. Comparison of daily river discharge during flood events in the catalogue, or a 30-day window centred around the dates of the event. Abbreviations are NUTS level 0 country codes. The graph shows the percentage of all stations per country by performance class: (a) KGE score; (b) Spearman's coefficient of determination.

598 **3.3.2 Extreme sea levels**

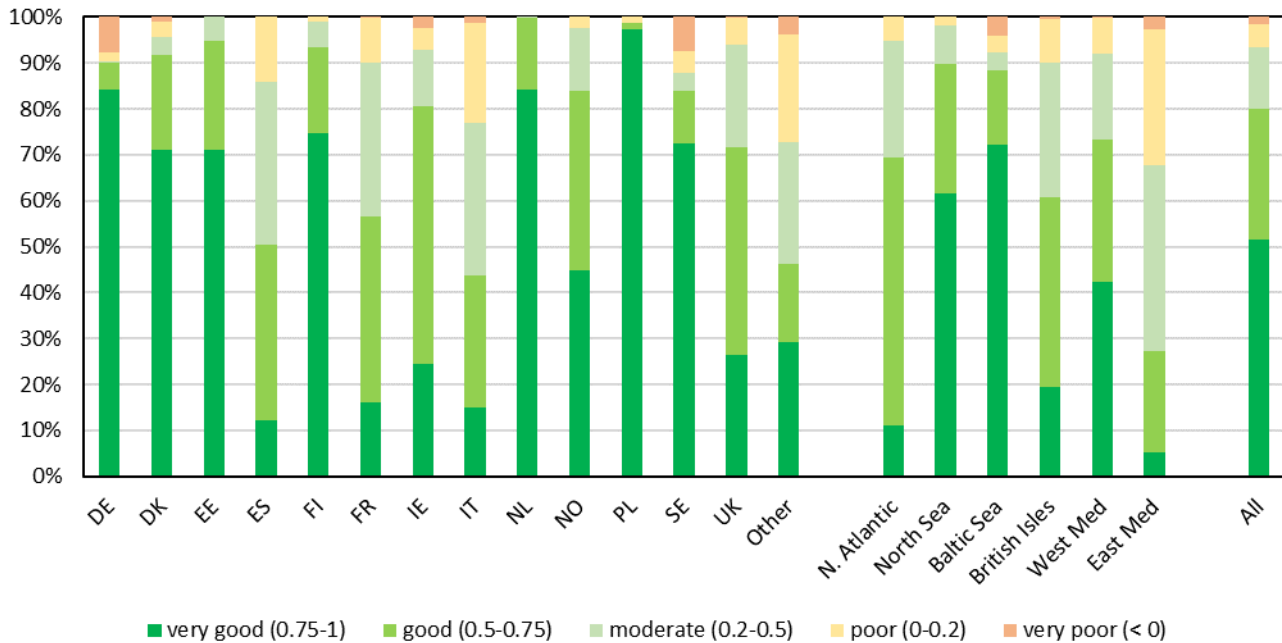
599 At least one tide gauge with adequate data length was available for 1363 events (56% of the total), and a total of 8102 time
600 series were identified within the NUTS3 regions potentially affected by those events. Most of the data is available for events
601 that have occurred in the United Kingdom, Denmark, Norway, the Netherlands, France, Sweden, and Germany. The overall
602 results are compared using several metrics in Table 7.6. Overall, the maximum sea levels observed during the various potential
603 coastal floods were well reproduced, with the main source of inaccuracies being storm surge heights. Further, 80% of modelled
604 time series spanning the duration of the events indicated a good or very good R^2 when compared with observations. For tides
605 and total water level, such performance was measured for 93–94% of stations. The best performance of the storm surge model
606 was recorded for North and Baltic seas (Fig. 4.12), with far lower performance for the Eastern Mediterranean Sea. However,
607 potential flood events and observational data are both relatively scarce in the latter region, which had the lowest scores also
608 for reproducing tides and combined sea level. As in the case of riverine events, there is little variation between events by
609 classification, though historical HANZE events (“A”) had slightly higher scores for storm surge heights and combined sea
610 level than all other classes. This could be, to some extent, the result of the difference in the geographical distribution of events.

611

612 **Table 7.6. Comparison between maximum hourly sea level and its components during flood events in the catalogue, or a 7-day**
613 **window centred around the dates of the event.**

Metric	Storm surge height	Tide elevation	Combined sea level
Pearson’s R^2	0.75	0.99	0.96
Spearman’s R^2	0.74	0.95	0.94
Nash-Sutcliffe Efficiency	0.47	0.99	0.96
Root mean squared error (RMSE) in metres	0.30	0.14	0.26
RMSE to standard deviation ratio	0.53	0.11	0.21

614



615

616

617

618

619

620

621

Figure 4.12. Comparison between maximum hourly storm surge height during flood events in the catalogue, or a 7-day window centred around the dates of the event. The graph shows the percentage of all stations per country by performance of Pearson's R^2 . Abbreviations in the left side of the graph are NUTS level 0 country codes. On the right side of the graph, stations are grouped by main European sea regions: "N. Atlantic" – exposed North Atlantic Ocean coasts (mostly France and Spain), "North Sea" – including Norwegian coasts, "Baltic Sea" – including Danish Straits, "British Isles" – coasts of Great Britain and Ireland, "West Med" and "East Med" – Western and Eastern Mediterranean Sea, respectively.

622

3.3.3 Comparison of flood footprints

623

624

625

626

627

628

629

630

631

632

633

634

Comparison of modelled potential flood impacts with impacts based on satellite-derived flood footprints and actual impacts recorded in the HANZE database highlights the challenge of correctly recreating past floods (Table 8.7). For exactly half of the 20 floods for which a satellite-derived footprint is available, our modelled population affected were closer to reported population affected than estimates based on satellite-derived flood footprints, and vice versa. In most cases, satellite-derived footprints severely underestimated the extent of the flooding, with the exception of floods in the United Kingdom, where they indicated many times more affected population than the reported actual impact. In all cases the modelled area and persons affected were higher than the actual impact, as was the intention of the catalogue, as modelled without flood protection. However, there is a very close match in persons affected during the August 2002 flood in Czechia and Germany. In the whole catalogue, the area affected was higher than reported in 83% of cases where the actual impact was reported in HANZE (i.e. 256 out of 307), fatalities in 98% of cases (1473 out of 1496), population affected in 89% of cases (686 out of 773) and economic loss in 89% of cases (675 out of 755).

635
636
637

Table 87. Comparison of modelled potential flood zone with satellite-derived footprints from the Global Flood Database (Tellman et al., 2021) and reported impacts from HANZE (Paprotny et al., 2023) for several European floods, 2002–2015. Area flooded in km². * percentage of the satellite flood footprint reproduced by the modelled flood footprint of this study.

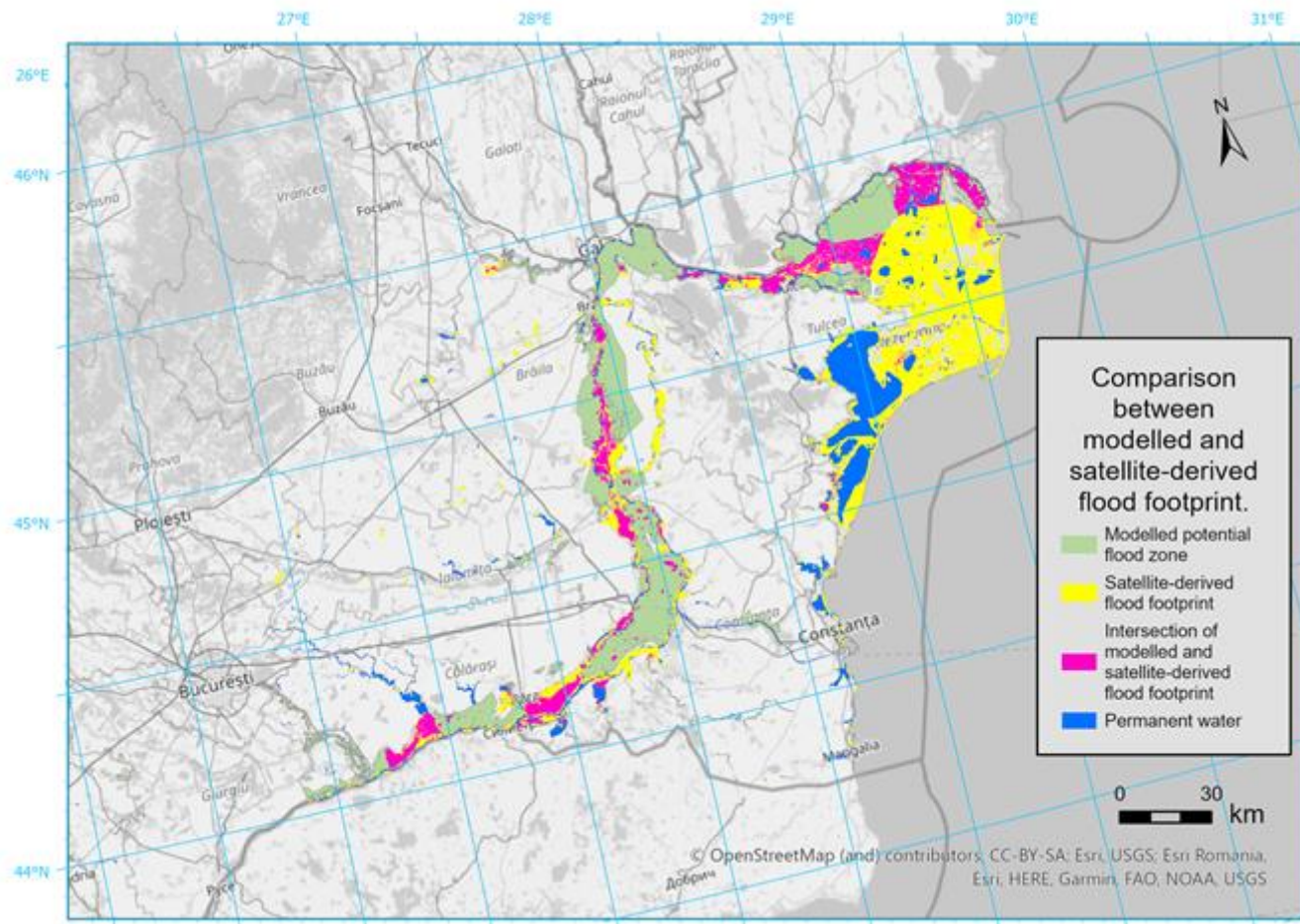
Event (country, month, year)	HANZ E ID	Reported impacts (HANZE)		Modelled impacts with potential flood zone		Modelled impacts with satellite footprints		Hit rate modelled area to satellite area*	Ratio of affected population	
		Area flooded	Persons affected	Area flooded	Persons affected	Area flooded	Persons affected		Modelled: reported	Reported: satellite
Albania, November/December 2010	2031	139	24,700	894	91,776	194	8,260	56%	3.7	3.0
Austria, March 2006	21		1,840	263	15,130	68	1,659	45%	8.2	1.1
Bosnia and Herzegovina, April-May 2004	2053	200	20,000	734	147,114	75	1,023	44%	7.4	19.6
Czechia, August 2002	86		225,000	1247	225,513	90	4,018	54%	1.0	56.0
France, September 2002	244		12,000	763	116,813	95	1,595	30%	9.7	7.5
France, December 2003	250		27,000	1,843	245,870	767	11,954	67%	9.1	2.3
Germany, August 2002	341		330,000	3,371	372,649	681	10,081	74%	1.1	32.7
Greece, January/February 2015	403	250	500	405	3,696	268	256	44%	7.4	2.0
Hungary, March-May 2006	421	2,440	5,400	5,201	310,750	918	10,886	37%	57.5	0.5
Hungary, May/June 2010	422	1,230	5,000	1,376	77,306	199	214	85%	15.5	23.3
Italy, November/December 2002	952		10,000	2,031	424,594	119	29,321	13%	42.5	2.9
Italy, January 2003	954		40,000	370	43,917	35	392	18%	1.1	102.0
Lithuania, March/April 2010	2200	400	2,000	1,211	27,851	214	464	59%	13.9	4.3
Montenegro, December 2010	2209		6,630	289	21,390	198	2,330	34%	3.2	2.8
Poland, May/June 2010	1065	5,540	280,000	7,151	775,536	348	9,757	71%	2.8	28.7
Romania, July 2005	1148	993	58,700	1,664	85,918	338	1,061	50%	1.5	55.3
Romania, April/May 2006	1153	1,165	15,011	5,305	115,330	3,415	6,626	43%	7.7	2.3
UK, November/December 2012	1558		4,400	1,156	132,320	869	265,903	12%	30.1	0.02
UK, December 2013-February 2014	1561	450	25,000	828	225,781	815	388,930	13%	9.0	0.06
UK, December 2015-January 2016	1563		64,000	1,016	100,633	1,472	480,026	9%	1.6	0.13

638

639
640

Direct comparison between modelled and satellite footprints (Fig. 4213) has shown that the hit rate, i.e. share of the satellite footprints correctly reproduced by the model, varied between 30 and 85%, except for events in Italy and the United Kingdom,

641 where it was only 9–18%. However, the satellite footprints also performed very poorly against reported losses for those floods.
642 Some additional flood events were analysed, but were not included in Table 6-7 as the satellite footprints showed virtually no
643 population affected, which is in large contrast to actual impacts. Such a situation occurred e.g. for the summer floods in the
644 United Kingdom in 2007 that flooded homes of about 192,000 people (HANZE database number 1546), almost none of which
645 could be reproduced with satellite flood footprints.
646



647
648 **Figure 1213.** Example comparison between modelled and satellite-derived flood footprint of the 2006 event in Romania.

649 **4 Discussion**

650 **4.1 Uncertainties and limitations of the models and modelled data**

651 The elaborate modelling chain involving both riverine and coastal processes is subject to multiple cascading limitations and
652 uncertainties. The starting point of the simulations are input climate data, derived from global reanalyses. Though ERA5 and

653 ERA5-Land are state-of-the-art, they still encounter problems of inhomogeneities, gaps or errors in observational data, model
654 biases, and limitations in representing precipitation extremes in particular (Hersbach et al., 2020, Muñoz-Sabater et al., 2021).
655 In the case of the riverine model, bias-adjustment and downscaling was carried out, but it is also only a statistical transformation
656 that depends on the quality of high-resolution observations as well (see section 4.1.2).
657 Validation results in section 3.1 indicate mostly good performance of the models in reconstructing past extreme discharges
658 and sea levels, but not in all areas. Some regions are more challenging to model than others, e.g. due to complex topography
659 or shoreline, or strong anthropogenic influence on the water cycle (especially through reservoirs). Not all types of floods or
660 processes that drive them could be represented. Most noticeably, the resolution of the riverine model is inadequate to capture
661 smaller flash floods, as the hydrological model has a spatial resolution of 1' driven by climate data that was twice downscaled
662 (first from ERA5 to ERA5-Land, then using ISIMIP3BASD method) and with a temporal resolution of six hours. Additionally,
663 flood hazard maps used to generate the footprints only covered catchments with an upstream area of at least 100 km².
664 Consequently, 91% of slow-onset riverine floods from HANZE were reproduced, but only 55% of flash floods. Urban floods
665 are not represented at all (also in the HANZE dataset).
666 Further, no flood defences are represented in the model, which is by design, as information on this aspect is scarce, especially
667 in the temporal dimension. At the same time, a flood that was historically prevented by existing defences might not have been
668 prevented under counterfactual conditions. We also hypothesise that flood protection levels are driven to some extent by flood
669 risk and flood occurrence (section 4.2). The use of flood hazard maps for a defined set of scenarios enables generating flood
670 footprints without carrying out a computationally infeasible continuous hydrodynamic simulation over a period of 71 years.
671 However, the maps assume a specific hydrograph which is not necessarily valid for all floods with the same peak discharge.
672 Further, the three sets of maps (including two sets for different catchment sizes) are methodologically different and were
673 created for diverse sets of scenarios. Whereas the coastal maps were rerun specifically for this study based on the results of
674 the extreme sea level modelling, the riverine maps are from previous studies. Their application is in some locations problematic
675 due to inconsistencies in river network delineation between EFAS and the hazard maps. The accuracy of the riverine flood
676 hazard maps is also variable depending on the region and the probability of occurrence (see Paprotny et al., 2017, and Dottori
677 et al., 2022, for details).
678 Compound floods are represented by merging riverine and coastal flood zones, which neglects the possible interaction between
679 the storm surge and river discharge that could generate higher water levels than is possible for individual drivers. Additionally,
680 not all coastal processes are included in the model, such as interaction between tide and storm surges, or influence of SLR on
681 tide elevations. Wave run-up is only approximated by taking one-fifth of offshore significant wave height, as more precise
682 estimates would require a very detailed model of the nearshore. Finally, long-term land motion is limited to GIA due to lack
683 of detailed data on the subject.

684 4.2 Uncertainties and limitations of the observations and documentary sources

685 The results are influenced not only by the accuracy of models, but also that of the observations. Our river discharge simulations
686 are driven by reanalysis data that were downscaled and bias-adjusted using interpolated meteorological observations, the
687 accuracy of which depends strongly on the density of point meteorological data. As shown in Thiemig et al. (2022),
688 precipitation during extreme events in the EMO dataset can at times diverge strongly from other reported measurements.
689 Though our meteorological input data is still driven primarily by ERA5, the reanalysis itself is influenced by availability of
690 meteorological data, which is very inhomogeneous in time (Hersbach et al., 2020). This might be the reason for the noticeably
691 lower performance of our model in reproducing flood events in the 1950s.

692 Model calibration and validation, as well as classification of the flood event catalogue is affected by the availability of tide
693 and river gauges (section 3.1.1 and 3.1.2). The data is unevenly distributed, with most data available for northern Europe,
694 particularly the Nordic countries and the British Isles. On the other hand, very limited data was available for Italy, Greece, and
695 Balkan countries. It is further uneven in time, with both the 1950s and the last few years until 2020 having lower coverage
696 than the 1990s and 2000s in particular. Identification of events as false positives (“E”) is also potentially problematic, as in
697 large NUTS3 regions the only available observations could be outside the impact zone of the event, hence incorrectly
698 suggesting that the model generated a ‘bogus’ event. Satellite-derived footprints were used to ~~validate~~ [compare](#) the modelled
699 flood footprints, but themselves often widely diverged from reported impacts. The hit rate between satellite and model data
700 varied significantly between individual events, similarly observed in a reconstruction of recent European coastal floods by Le
701 Gal et al. (2023).

702 Similarly, documentary sources on socioeconomic impacts of floods are highly uneven in quality between countries. For
703 instance, while there are comprehensive databases and flood catalogues accessible e.g. for France, Italy, Norway, Portugal,
704 Spain, or Switzerland, and even some Balkan countries, scattering of information makes it very laborious to collect data for
705 other countries, e.g. Austria, Germany, and the United Kingdom. Many compilations of flood impacts only cover the recent
706 two decades, while older flood catalogues published in the 1980s or 1990s often have no newer follow-ups. This strongly
707 affects the frequency of “C” (No impacts) events relative to “D” (Impacts unknown). Thanks to extensive research in the
708 HANZE database, this has less effect on detection of “A” (Impacts, data) and “B” (Impacts, no data) events. Still, uncertainty
709 surrounds designation of flood events as having “significant” socioeconomic impacts. The thresholds defined in HANZE are
710 somewhat arbitrary, though based on experience of collecting more than 2500 records in the dataset. In case of smaller events,
711 their classification is uncertain if the data is incomplete or not very accurate. This is potentially problematic for “B” events,
712 where at times no quantitative data at all is available, and the classification was based on the description of impacts only.
713 Finally, NUTS3 regions, the principal socioeconomic unit of observation here and in HANZE, vary in size both in terms of
714 area and population. It might be slightly easier for floods in large regions to pass region-scale threshold for minimum flood
715 area in the model, and to be considered affected in HANZE, where region-scale impact thresholds are also applied when
716 detailed damage data are available.

717 5 Conclusions

718 This study is the largest attempt to reconstruct past flood losses in Europe, and makes an advance towards full decomposition
719 of drivers of historical flood losses. We created a flood catalogue for Europe containing 14,699 events with significant
720 socioeconomic impact potential. It covers riverine, coastal and compound events over a period of 71 years, and considers
721 climate change, evolving human impact on catchments, and growing exposure. [However, it should be highlighted that the
722 damage estimates provided in the catalogue exclude the influence of flood defences, and spatial and temporal variation of
723 vulnerability levels.](#)

724 The catalogue includes 1504 out of 2037 damaging floods since 1950 included in HANZE dataset (Paprotny et al., 2023),
725 including some 90% of coastal, compound and slow-onset riverine floods, and 55% of flash floods. The coverage of reported
726 impacts of those events is 81-99% depending on the exact measure. The performance of the model is relatively stable over
727 time, though slightly worse for the 1950s.

728 The flood catalogue was primarily devised as the baseline (factual) reconstruction of past floods in Europe. However, it can
729 be also used directly for multiple applications. The immediate follow-up to this analysis will be modelling changes in flood
730 preparedness in Europe in the past 70 years, including flood protection standards and relative losses (~~vulnerability~~[Paprotny et
731 al., 2024](#)). The modelling chain can be further used with counterfactual climate inputs. Methods such as ATTRICI (Mengel et
732 al., 2021) enable removing the global warming effect from all variables required to model riverine discharges. Additional
733 counterfactual simulations are possible to quantify the human influence on catchments, particularly through construction of
734 reservoirs (Boulangé et al., 2021). Methods such as transformed-stationary extreme value analysis (Mentaschi et al., 2016) can
735 be used to detrend storm surge heights in addition to removing the long-term sea level rise. Together with HANZE historical
736 exposure maps (Paprotny and Mengel, 2023), counterfactual scenarios for all components of risk would be achieved. This
737 would provide the first comprehensive impact attribution of European flood losses and generate an important reference dataset
738 for pan-European flood risk assessments.

739

740 *Data & code availability:* Numerous public datasets and models were used in the study, results of which are also publicly
741 available. Details where to find each dataset and model are provided in Appendix A3. [The flood event catalogue is also
742 accessible through <https://naturalhazards.eu/>.](#)

743 *Code availability:* [The main code for generating the flood catalogue is available from Zenodo
744 \(<https://doi.org/10.5281/zenodo.10678820>\). More links to other models and code are provided in Appendix A3.](#)

745 *Author contributions.* DP developed the concept, implemented the methods, collected and processed most of the data, and
746 acquired funding. BR collected part of the historical impact data and performed part of the flood event classification. MV
747 computed coastal flood hazard maps. PT and JS performed the ~~validation-comparison~~ based on satellite-derived flood
748 footprints and created the online visualisation of the study. FD and ST contributed datasets and methods for the riverine and
749 coastal simulations, respectively. LF and HK helped to develop the concept and methods. All authors wrote the paper.

750 *Competing interests.* The authors declare that they have no conflict of interest.

751 *Financial support.* This research has been supported by the German Research Foundation (DFG) through project
752 “Decomposition of flood losses by environmental and economic drivers” (FloodDrivers), grant no. 449175973.

753 **Appendix A1. Contents of “B” list of historical floods**

754 The format of the database of “B” list events follows the same format of HANZE database (Paprotny et al., 2023), with a
755 reduced number of fields as events were confined to the “B” list specifically due to lack of relevant data (primarily flood
756 impact statistics). Most fields have strictly-defined permitted values, except “Notes”, which includes explanation why impacts
757 should be considered significant (using partial available data or descriptive indicators), and “Data sources” which lists all cited
758 references. The latter are often the same as used in the HANZE database, therefore only publications specific to the B list are
759 included in the full bibliographic details provided with the event file. For detailed discussion about the contents of each field
760 we refer to Paprotny et al. (2023).

761
762 **Table A1. Summary of fields recorded in the “B” list of floods.**

Variable	Short description	Field type	Permitted values
ID	Unique event identifier	integer	7000...8999
Country code	Two-letter country code	string	Codes from Table B1
Year	Year of the event	integer	1950...2020
Country name	Country name	string	Names from Table B1
Start date	Daily start date	date	1.1.1950...31.12.2020
End date	Daily end date	date	1.1.1950...31.01.2021
Type	Detailed type of event	string	River, Flash, Coastal, River/Coastal
Regions affected (NUTS3 v2010)	Regions where human or economic losses were reported, at NUTS3 level (version 2010)	string	Codes from Table B2
Regions affected (NUTS3 v2021)	As above, but at using NUTS version 2021	string	Codes from Table B3
Notes	Other relevant information or notes on issues with the data	string	Free text
References	List of publications and databases from which the information was obtained	string	Free text

763

764

Variable	Short description
ID	Unique event identifier
Country code	Two-letter country code
Year	Year of the event
Country name	Country name
Start date	Daily start date
End date	Daily end date
Type	Detailed type of event
Flood source	Rivers or sea basins in the potentially-affected area (from Vogt et al., 2007, and Fourcy and Lorvelec, 2013)
Regions affected (NUTS3 v2010)	Regions where human or economic losses were reported, at NUTS3 level (version 2010)
Regions affected (NUTS3 v2021)	As above, but at using NUTS version 2021
Area inundated	Potential inundated area in hectares (ha)
Fatalities, YE	Potential fatalities, in persons, year-of-event exposure
Fatalities, 1950	Potential fatalities, in persons, 1950 exposure
Fatalities, 2020	Potential fatalities, in persons, 2020 exposure
Persons affected, YE	Potential persons affected, in persons, year-of-event exposure
Persons affected, 1950	Potential persons affected, in persons, 1950 exposure
Persons affected, 2020	Potential persons affected, in persons, 2020 exposure
Economic loss, YE	Potential direct economic loss, in thousands of 2020 euros, year-of-event exposure
Economic loss, 1950	Potential direct economic loss, in thousands of 2020 euros, 1950 exposure
Economic loss, 2020	Potential direct economic loss, in thousands of 2020 euros, 2020 exposure
Loss threshold	Threshold for direct economic losses applied to the event, in thousands of 2020 euros
Mean water depth	Average water depth in the potential inundated zone
Return period	Average (geometric) of return periods along potential affected river grid cells or coastal segments, from detrended 1950–2020 data, Generalised Pareto distribution
Hydro data	Indicates if river or tide gauge data were available for this event (1 – yes, 0 – no)
RP2 exceedance	Indicates if a 2-year return period was exceeded in the observational data (1 – yes, 0 – no)
Category	Classification of event according to Table 43
HANZE ID	Flood event ID if event classified as “A” or “B”, otherwise empty field

Table A3. Availability of input and output data and models from the study. Models are indicated by *italics*.

Variable, data	Dataset/ <i>model</i>	Resource link
River discharges	HERA	https://data.jrc.ec.europa.eu/dataset/a605a675-9444-4017-8b34-d66be5b18c95
Meteorological data for storm surge simulation, significant wave height	ERA5	https://doi.org/10.24381/cds.e2161bac
<i>Hydrodynamic model (coastal)</i>	<i>Delft3D</i>	https://oss.deltares.nl/web/delft3d/get-started
Tide elevation constituents	FES2014	https://www.aviso.altimetry.fr/en/data/products/auxiliary-products/global-tide-fes.html
<i>Tide elevation model</i>	<i>pyTMD</i>	https://github.com/tsutterley/pyTMD
Mean dynamic topography	Global Ocean Mean Dynamic Topography	https://doi.org/10.48670/moi-00150
Sea level rise	Hourly Coastal water levels with Counterfactual	https://zenodo.org/records/7771386
Sea level rise	European Seas Gridded L 4 Sea Surface Heights	https://doi.org/10.48670/moi-00141
Sea level rise	Global Ocean Gridded L 4 Sea Surface Heights	https://doi.org/10.48670/moi-00148
Glacial isostatic adjustment	ICE-6G_C	https://www.atmosp.physics.utoronto.ca/~peltier/data.php
Storm surge heights, combined water level, tide levels	This study	https://doi.org/10.5281/zenodo.10630338
DEM for coastal inundation	GLO-30	https://doi.org/10.5069/G9028PQB
<i>Hydrodynamic model for coastal inundation</i>	<i>Lisflood-ACC</i>	https://www.seamlesswave.com/LISFLOOD8.0
Land use and population at 100 m resolution	HANZE v2.0 output maps	https://doi.org/10.5281/zenodo.7885990
<i>Exposure model (population, fixed assets by sector)</i>	<i>HANZE v2.0</i>	https://doi.org/10.5281/zenodo.7556953
Historical flood impacts (“A” list) and list of references	HANZE v2.1	https://doi.org/10.5281/zenodo.8410025 https://doi.org/10.5281/zenodo.11259233
Significant flood events without direct impact data (“B” list)	This study	https://doi.org/10.5281/zenodo.10629443 https://doi.org/10.5281/zenodo.10949631
List of documentary sources used	This study	https://doi.org/10.5281/zenodo.10629443 https://doi.org/10.5281/zenodo.10949631
Coastal flood hazard maps, flood catalogue input data	This study	https://doi.org/10.5281/zenodo.10630862
River flood hazard maps	JRC maps	https://doi.org/10.2905/1D128B6C-A4EE-4858-9E34-6210707F3C81
River flood hazard maps	RAIN project maps	https://doi.org/10.4121/uuid:968098ce-afe1-4b21-a509-dedaf9bf4bd5
Historical flood database	EM-DAT	https://public.emdat.be/
Historical flood database	EEA Flood Phenomena	https://www.eea.europa.eu/data-and-maps/data/european-past-floods/flood-phenomena
Historical flood database	Dartmouth Flood Observatory	http://floodobservatory.colorado.edu/Archives/index.html
Historical flood database	FFEM-DB	https://doi.org/10.4121/14754999.v2
Historical flood database	Recorded Flood Outlines	https://www.data.gov.uk/dataset/16e32c53-35a6-4d54-a111-ca09031eaaaf/recorded-flood-outlines
River discharge data	GRDC	https://portal.grdc.bafg.de/
River discharge data (France)	HydroPortail	https://www.hydro.eaufrance.fr/rechercher/entites-hydrometriques

River discharge data (Norway)	NVE, Historiske vannføringsdata til produksjonsplanlegging	https://www.nve.no/vann-og-vassdrag/hydrologiske-data/historiske-data/historiske-vannfoeringsdata-til-produksjonsplanlegging/
River discharge data (Spain)	Centro de Estudios Hidrográficos, Anuario de aforos	https://ceh.cedex.es/anuarioaforos/default.asp
River discharge data (Sweden)	SMHI Vattenwebb	https://www.smhi.se/data/hydrologi/vattenwebb
River discharge data (UK)	UK National River Flow Archive	https://nrfa.ceh.ac.uk/
River discharge, sea level data (Poland)	IMGW-PIB, Dane Publiczne	https://danepubliczne.imgw.pl/
Sea level data	GESLA v3	https://gesla787883612.wordpress.com/
Sea level data	Poseidon System	https://poseidon.hcmr.gr/services/ocean-data/situ-data
Satellite flood footprints	Global Flood Database	https://global-flood-database.cloudtostreet.ai/#interactive-map
<i>Flood catalogue generation model</i>	<i>This study</i>	https://doi.org/10.5281/zenodo.10678820
Modelled flood catalogue	This study	https://doi.org/10.5281/zenodo.10629443 https://doi.org/10.5281/zenodo.10949631
Modelled flood footprints	This study	https://doi.org/10.5281/zenodo.10640692 https://doi.org/10.5281/zenodo.10943896

771

772

References

773

[Andreadis, K. M., O. E. Wing, E. Colven, C. J. Gleason, P. D. Bates, and C. M. Brown. 2022. Urbanizing the floodplain: Global changes of imperviousness in flood-prone areas, *Environ. Res. Lett.*, 17, 104024. <https://doi.org/10.1088/1748-9326/ac9197>, 2022.](#)

774

775

Argus, D.F., Peltier, W.R., Drummond, R., and Moore, A.W.: The Antarctica component of postglacial rebound model ICE-6G_C (VM5a) based upon GPS positioning, exposure age dating of ice thicknesses, and relative sea level histories, *Geophys. J. Int.*, 198, 537-563, <https://doi.org/10.1093/gji/ggu140>, 2014.

779

Arnal, L., Asp, S.-S., Baugh, C., de Roo, A., Disperati, J., Dottori, F., Garcia, R., Garcia Padilla, M., Gelati, E., Gomes, G., Kalas, M., Krzeminski, B., Latini, M., Lorini, V., Mazzetti, C., Mikulickova, M., Muraro, D., Prudhomme, C., Rauthe-Schöch, A., Rehfeldt, K., Salamon, P., Schweim, C., Skoien, J. O., Smith, P., Sprokkereef, E., Thiemig, V., Wetterhall, F., and Ziese, M.: EFAS upgrade for the extended model domain – technical documentation, Publications Office of the European Union, Luxembourg, <https://doi.org/10.2760/806324>, 2019.

784

Bates, P. D., Horritt, M. S., and Fewtrell, T. J.: A simple inertial formulation of the shallow water equations for efficient two-dimensional flood inundation modelling, *J. Hydrol.*, 387, 33–45, <https://doi.org/10.1016/j.jhydrol.2010.03.027>, 2010.

786

Batista e Silva, F., Lavallo, C., and Koomen, E.: A procedure to obtain a refined European land use/cover map, *J. Land Use Sci.*, 8, 255–283, <https://doi.org/10.1080/1747423X.2012.667450>, 2012.

788

Bednar-Friedl, B., Biesbroek, R., Schmidt, D.N., Alexander, P., Børshheim, K. Y., Carnicer, J., Georgopoulou, E., Haasnoot, M., Le Cozannet, G., Lionello, P., Lipka, O., Möllmann, C., Muccione, V., Mustonen, T., Piepenburg, D., and Whitmarsh, L.:

789

790 Europe, *Climate Change 2022: Impacts, Adaptation and Vulnerability, Contribution of Working Group II to the Sixth*
791 *Assessment Report of the Intergovernmental Panel on Climate Change*, Cambridge University Press, Cambridge, UK and New
792 York, NY, USA, 1817–1927, <https://doi.org/10.1017/9781009325844.015>, 2022.

793 Blöschl, G., Kiss, A., Viglione, A., Barriendos, M., Böhm, O., Brázdil, R., Coeur, D., Demarée, G., Llasat, M. C., Macdonald,
794 N., Retsö, D., Roald, L., Schmockler-Fackel, P., Amorim, I., Belinová, M., Benito, G., Bertolin, C., Camuffo, D., Cornel, D.,
795 Doctor, R., Elleder, L., Enzi, S., Garcia, J. C., Glaser, R., Hall, J., Haslinger, K., Hofstätter, M., Komma, J., Limanówka, D.,
796 Lun, D., Panin, A., Parajka, J., Petric, H., Rodrigo, F. S., Rohr, C., Schönbein, J., Schulte, L., Silva, L. P., Toonen, W., Valent,
797 P., Waser, J., and Wetter, O.: Current flood-rich period is exceptional compared to the past 500 years in Europe, *Nature*, 583,
798 560–566, <https://doi.org/10.1038/s41586-020-2478-3>, 2020.

799 Boulange, J., Hanasaki, N., Yamazaki, D., and Pokhrel, Y.: Role of dams in reducing global flood exposure under climate
800 change, *Nat Commun.*, 12, 417, <https://doi.org/10.1038/s41467-020-20704-0>, 2021.

801 Boyd, E., Levitan, M., and van Heerden, I.: Further specification of the dose-response relationship for flood fatality estimation,
802 paper presented at the US-Bangladesh workshop on innovation in windstorm/storm surge mitigation construction, National
803 Science Foundation and Ministry of Disaster & Relief, Government of Bangladesh, Dhaka, 19–21 December 2005.

804 Brakenridge, G. R.: Global Active Archive of Large Flood Events. Dartmouth Flood Observatory, University of Colorado,
805 available at <http://floodobservatory.colorado.edu/Archives/index.html> (last access: 26 October 2023), 2023.

806 Burek, P., van der Knijff, J., and De Roo, A.: LISFLOOD - Distributed Water Balance and Flood Simulation Model - Revised
807 User Manual 2013, Publications Office of the European Union, Luxembourg, <https://doi.org/10.2788/24982>, 2013.

808 Centre for Research on the Epidemiology of Disasters: EM-DAT, CRED / UCLouvain, Brussels, Belgium,
809 <https://www.emdat.be/> (last access: 26 October 2023), 2023.

810 Choulga, M., Moschini, F., Mazzetti, C., Grimaldi, S., Disperati, J., Beck, H., Salamon, P., and Prudhomme, C.: Technical
811 note: Surface fields for global environmental modelling, *EGUsphere* [preprint], <https://doi.org/10.5194/egusphere-2023-1306>,
812 2023.

813 Copernicus Emergency Management Service: European Flood Awareness System (EFAS) version 5.0, available at
814 <https://confluence.ecmwf.int/display/CEMS/European+Flood+Awareness+System> (last access: 8 November 2023), 2023.

815 Diederer, D., Liu, Y., Gouldby, B., Diermanse, F., and Vorogushyn, S.: Stochastic generation of spatially coherent river
816 discharge peaks for continental event-based flood risk assessment, *Nat. Hazards Earth Syst. Sci.*, 19, 1041–1053,
817 <https://doi.org/10.5194/nhess-19-1041-2019>, 2019.

818 Dottori, F., Alfieri, L., Bianchi, A., Skoien, J., and Salamon, P.: A new dataset of river flood hazard maps for Europe and the
819 Mediterranean Basin, *Earth Syst. Sci. Data*, 14, 1549–1569, <https://doi.org/10.5194/essd-14-1549-2022>, 2022.

820 Enríquez, A. R., Wahl, T., Marcos, M., and Haigh, I. D.: Spatial footprints of storm surges along the global coastlines, *J.*
821 *Geophys. Res.-Oceans*, 125, e2020JC016367, <https://doi.org/10.1029/2020JC016367>, 2020.

822 Environment Agency: Recorded Flood Outlines, available at [https://www.data.gov.uk/dataset/16e32c53-35a6-4d54-a111-](https://www.data.gov.uk/dataset/16e32c53-35a6-4d54-a111-ca09031eaaaf/recorded-flood-outlines)
823 [ca09031eaaaf/recorded-flood-outlines](https://www.data.gov.uk/dataset/16e32c53-35a6-4d54-a111-ca09031eaaaf/recorded-flood-outlines) (last access: 31 October 2023), 2023.

824 European Environment Agency: Flood phenomena, available at [https://www.eea.europa.eu/data-and-maps/data/european-](https://www.eea.europa.eu/data-and-maps/data/european-past-floods/flood-phenomena)
825 [past-floods/flood-phenomena](https://www.eea.europa.eu/data-and-maps/data/european-past-floods/flood-phenomena) (last access: 26 October 2023), 2015.

826 European Space Agency and Sinergise: Copernicus Global Digital Elevation Model, OpenTopography [dataset],
827 <https://doi.org/10.5069/G9028PQB>, 2021.

828 Eurostat: Statistical regions in the European Union and partner countries NUTS and statistical regions 2021 - re-edition 2022,
829 Publications Office of the European Union, Luxembourg, <https://doi.org/10.2785/321792>, 2022.

830 Fourcy, D., and Lorvelec, O.: A new digital map of limits of oceans and seas consistent with high-resolution global shorelines,
831 *J. Coast. Res.*, 29, 471–477, <http://dx.doi.org/10.2112/JCOASTRES-D-12-00079.1>, 2013.

832 Frieler, K., Volkholz, J., Lange, S., Schewe, J., Mengel, M., del Rocío Rivas López, M., Otto, C., Reyer, C. P. O., Karger, D.
833 N., Malle, J. T., Treu, S., Menz, C., Blanchard, J. L., Harrison, C. S., Petrik, C. M., Eddy, T. D., Ortega-Cisneros, K., Novaglio,
834 C., Rousseau, Y., Watson, R. A., Stock, C., Liu, X., Heneghan, R., Tittensor, D., Maury, O., Büchner, M., Vogt, T., Wang, T.,
835 Sun, F., Sauer, I. J., Koch, J., Vanderkelen, I., Jägermeyr, J., Müller, C., Rabin, S., Klar, J., Vega del Valle, I. D., Lasslop, G.,
836 Chadburn, S., Burke, E., Gallego-Sala, A., Smith, N., Chang, J., Hantson, S., Burton, C., Gädeke, A., Li, F., Gosling, S. N.,
837 Müller Schmied, H., Hattermann, F., Wang, J., Yao, F., Hickler, T., Marcé, R., Pierson, D., Thiery, W., Mercado-Bettín, D.,
838 Ladwig, R., Ayala-Zamora, A. I., Forrest, M., and Bechtold, M.: Scenario setup and forcing data for impact model evaluation
839 and impact attribution within the third round of the Inter-Sectoral Model Intercomparison Project (ISIMIP3a), *Geosci. Model*
840 *Dev.*, 17, 1–51, <https://doi.org/10.5194/gmd-17-1-2024>, 2024.

841 Ganguli, P., Paprotny, D., Hasan, M., Güntner, A., Merz, B.: Projected changes in compound flood hazard from riverine and
842 coastal floods in Northwestern Europe, *Earth’s Future*, 8, e2020EF001752, <https://doi.org/10.1029/2020EF001752>, 2020.

843 Haigh, I. D., Marcos, M., Talke, S. A., Woodworth, P. L., Hunter, J. R., and Hague, B. S.: GESLA Version 3: A major update
844 to the global higher-frequency sea-level dataset, *Geosci. Data J.*, 10, 293–314, <https://doi.org/10.1002/gdj3.174>, 2023.

845 Hersbach, H., Bell, B., Berrisford, P., et al.: The ERA5 global reanalysis, *Q. J. R. Meteorol. Soc.*, 146, 1999–2049,
846 <https://doi.org/10.1002/qj.3803>, 2020.

847 Huizinga, J., de Moel, H., Szwedczyk, W.: Global flood depth-damage functions. Methodology and the database with
848 guidelines, Publications Office of the European Union, Luxembourg, <https://doi.org/10.2760/16510>, 2017.

849 Institute of Meteorology and Water Management – National Research Institute: Dane publiczne. Available at:
850 <https://danepubliczne.imgw.pl/> (last access: 11 November 2023), 2023.

851 Jacob, D., Petersen, J., Eggert, B. et al.: EURO-CORDEX: new high-resolution climate change projections for European
852 impact research, *Reg. Environ. Change*, 14, 563–578, <https://doi.org/10.1007/s10113-013-0499-2>, 2014.

853 Jones, P. W.: First- and Second-Order Conservative Remapping Schemes for Grids in Spherical Coordinates, *Mon. Weather*
854 *Rev.*, 127, 2204–2210, [https://doi.org/10.1175/1520-0493\(1999\)127<2204:FASOCR>2.0.CO;2](https://doi.org/10.1175/1520-0493(1999)127<2204:FASOCR>2.0.CO;2), 1999.

855 Jonkman, S. N., Vrijling, J. K., and Vrouwenvelder, A. C. W. M.: Methods for the estimation of loss of life due to floods: a
856 literature review and a proposal for a new method, *Nat. Hazards*, 46, 353–389, <https://doi.org/10.1007/s11069-008-9227-5>,
857 2008.

858 Klein Goldewijk, K., Beusen, A., Doelman, J., and Stehfest, E.: Anthropogenic land use estimates for the Holocene – HYDE
859 3.2, *Earth Syst. Sci. Data*, 9, 927–953, <https://doi.org/10.5194/essd-9-927-2017>, 2017.

860 Kreibich, H., Blauhut, V., Aerts, J. C. J. H., Bouwer, L. M., Van Lanen, H. A. J., Mejia, A., Mens, M., and Van Loon, A. F.:
861 How to improve attribution of changes in drought and flood impacts, *Hydrolog. Sci. J.*, 64, 1–18,
862 <https://doi.org/10.1080/02626667.2018.1558367>, 2019.

863 Kreibich, H., Schröter, K., Di Baldassarre, G., Van Loon, A. F., Mazzoleni, M., Abeshu, G. W., Agafonova, S., AghaKouchak,
864 A., Aksoy, H., Alvarez-Garreton, C., Aznar, B., Balkhi, L., Barendrecht, M. H., Biancamaria, S., Bos-Burgering, L., Bradley,
865 C., Budiyono, Y., Buytaert, W., Capewell, L., Carlson, H., Cavus, Y., Couasnon, A., Coxon, G., Daliakopoulos, I., de Ruiter,
866 M. C., Delus, C., Erfurt, M., Esposito, G., François, D., Frappart, F., Freer, J., Frolova, N., Gain, A. K., Grillakis, M., Grima,
867 J. O., Guzmán, D. A., Huning, L. S., Ionita, M., Kharlamov, M., Khoi, D. N., Kieboom, N., Kireeva, M., Koutroulis, A.,
868 Lavado-Casimiro, W., Li, H.-Y., Llasat, M. C., Macdonald, D., Mård, J., Mathew-Richards, H., McKenzie, A., Mejia, A.,
869 Mendiondo, E. M., Mens, M., Mobini, S., Mohor, G. S., Nagavciuc, V., Ngo-Duc, T., Nguyen, H. T. T., Nhi, P. T. T., Petrucci,
870 O., Quan, N. H., Quintana-Seguí, P., Razavi, S., Ridolfi, E., Riegel, J., Sadik, M. S., Sairam, N., Savelli, E., Sazonov, A.,
871 Sharma, S., Sörensen, J., Souza, F. A. A., Stahl, K., Steinhausen, M., Stoelzle, M., Szalińska, W., Tang, Q., Tian, F.,
872 Tokarczyk, T., Tovar, C., Tran, T. V. T., van Huijgevoort, M. H. J., van Vliet, M. T. H., Vorogushyn, S., Wagener, T., Wang,
873 Y., Wendt, D. E., Wickham, E., Yang, L., Zambrano-Bigiarini, M., and Ward, P. J.: Panta Rhei benchmark dataset: socio-
874 hydrological data of paired events of floods and droughts, *Earth Syst. Sci. Data*, 15, 2009–2023, [https://doi.org/10.5194/essd-](https://doi.org/10.5194/essd-15-2009-2023)
875 [15-2009-2023](https://doi.org/10.5194/essd-15-2009-2023), 2023.

876 Kreibich, H., Van Loon, A. F., Schröter, K., Ward, P. J., Mazzoleni, M., Sairam, N., Abeshu, G. W., Agafonova, S.,
877 AghaKouchak, A., Aksoy, H., Alvarez-Garreton, C., Aznar, B., Balkhi, L., Barendrecht, M. H., Biancamaria, S., Bos-
878 Burgering, L., Bradley, C., Budiyono, Y., Buytaert, W., Capewell, L., Carlson, H., Cavus, Y., Couasnon, A., Coxon, G.,
879 Daliakopoulos, I., de Ruiter, M. C., Delus, C., Erfurt, M., Esposito, G., François, D., Frappart, F., Freer, J., Frolova, N., Gain,
880 A. K., Grillakis, M., Grima, J. O., Guzmán, D. A., Huning, L. S., Ionita, M., Kharlamov, M., Khoi, D. N., Kieboom, N.,
881 Kireeva, M., Koutroulis, A., Lavado-Casimiro, W., Li, H., Llasat, M. C., Macdonald, D., Mård, J., Mathew-Richards, H.,
882 McKenzie, A., Mejia, A., Mendiondo, E. M., Mens, M., Mobini, S., Mohor, G. S., Nagavciuc, V., Ngo-Duc, T., Nguyen, H.
883 T. T., Nhi, P. T. T., Petrucci, O., Quan, N. H., Quintana-Seguí, P., Razavi, S., Ridolfi, E., Riegel, J., Sadik, M. S., Savelli, E.,
884 Sazonov, A., Sharma, S., Sörensen, J., Souza, F. A. A., Stahl, K., Steinhausen, M., Stoelzle, M., Szalińska, W., Tang, Q., Tian,
885 F., Tokarczyk, T., Tovar, C., Tran, T. V. T., Van Huijgevoort, M. H. J., van Vliet, M. T. H., Vorogushyn, S., Wagener, T.,
886 Wang, Y., Wendt, D. E., Wickham, E., Yang, L., Zambrano-Bigiarini, M., Blöschl, G., and Di Baldassarre, G.: The challenge
887 of unprecedented floods and droughts in risk management, *Nature*, 608, 80–86, <https://doi.org/10.1038/s41586-022-04917-5>,
888 2022.

889 Lange, S.: Trend-preserving bias adjustment and statistical downscaling with ISIMIP3BASD (v1.0), *Geosci. Model Dev.*, 12,
890 3055–3070, <https://doi.org/10.5194/gmd-12-3055-2019>, 2019.

891 Lange, S.: ISIMIP3BASD (3.0.0), Zenodo [code], <https://doi.org/10.5281/zenodo.6501284>, 2022.

892 Le Gal, M., Fernández-Montblanc, T., Duo, E., Montes Perez, J., Cabrita, P., Souto Ceccon, P., Gastal, V., Ciavola, P., and
893 Armaroli, C.: A new European coastal flood database for low–medium intensity events, *Nat. Hazards Earth Syst. Sci.*, 23,
894 3585–3602, <https://doi.org/10.5194/nhess-23-3585-2023>, 2023.

895 Lehner, B., Reidy Liermann, C., Revenga, C., Vörösmarty, C., Fekete, B., Crouzet, P., Döll, P., Endejan, M., Frenken, K.,
896 Magome, J., Nilsson, C., Robertson, J. C., Rodel, R., Sindorf, N., and Wisser, D.: High-resolution mapping of the world’s
897 reservoirs and dams for sustainable river-flow management, *Front. Ecol. Environ.*, 9, 494–502, <https://doi.org/10.1890/100125>,
898 2011.

899 Lyard, F. H., Allain, D. J., Cancet, M., Carrère, L., and Picot, N.: FES2014 global ocean tide atlas: design and performance,
900 *Ocean Sci.*, 17, 615–649, <https://doi.org/10.5194/os-17-615-2021>, 2021.

901 Mengel, M., Treu, S., Lange, S., and Frieler, K.: ATTRICI v1.1 – counterfactual climate for impact attribution, *Geosci. Model*
902 *Dev.*, 14, 5269–5284, <https://doi.org/10.5194/gmd-14-5269-2021>, 2021.

903 Mentaschi, L., Vousdoukas, M., Voukouvalas, E., Sartini, L., Feyen, L., Besio, G., and Alfieri, L.: The transformed-stationary
904 approach: a generic and simplified methodology for non-stationary extreme value analysis, *Hydrol. Earth Syst. Sci.*, 20, 3527–
905 3547, <https://doi.org/10.5194/hess-20-3527-2016>, 2016.

906 Merz, B., Blöschl, G., Vorogushyn, S., Dottori, F., Aerts, J. C., Bates, P., Bertola, M., Kemter, M., Kreibich, H., and Lall, U.:
907 Causes, impacts and patterns of disastrous river floods, *Nature Reviews Earth & Environment*, 2, 592–609,
908 <https://doi.org/10.1038/s43017-021-00195-3>, 2021.

909 Mester, B., Frieler, K., and Schewe, J.: Human displacements, fatalities, and economic damages linked to remotely observed
910 floods, *Sci. Data*, 10, 482, <https://doi.org/10.1038/s41597-023-02376-9>, 2023.

911 Muis, S., Apecechea, M. I., Dullaart, J., de Lima Rego, J., Madsen, K. S., Su, J., Yan, K., and Verlaan, M.: A High-resolution
912 global dataset of extreme sea levels, tides, and storm surges, including future projections, *Frontiers in Marine Science*, 7, 263,
913 <https://doi.org/10.3389/fmars.2020.00263>, 2020.

914 Mulet, S., Rio, M.-H., Etienne, H., Artana, C., Cancet, M., Dibarboure, G., Feng, H., Husson, R., Picot, N., Provost, C., and
915 Strub, P. T.: The new CNES-CLS18 global mean dynamic topography, *Ocean Sci.*, 17, 789–808, [https://doi.org/10.5194/os-](https://doi.org/10.5194/os-17-789-2021)
916 [17-789-2021](https://doi.org/10.5194/os-17-789-2021), 2021.

917 Muñoz-Sabater, J., Dutra, E., Agustí-Panareda, A., Albergel, C., Arduini, G., Balsamo, G., Boussetta, S., Choulga, M.,
918 Harrigan, S., Hersbach, H., Martens, B., Miralles, D. G., Piles, M., Rodríguez-Fernández, N. J., Zsoter, E., Buontempo, C.,
919 and Thépaut, J.-N.: ERA5-Land: a state-of-the-art global reanalysis dataset for land applications, *Earth Syst. Sci. Data*, 13,
920 4349–4383, <https://doi.org/10.5194/essd-13-4349-2021>, 2021.

921 Nicholls, R. J., Lincke, D., Hinkel, J., Brown, S., Vafeidis, A. T., Meyssignac, B., Hanson, S. E., Merkens, J. L., and Fang, J.:
922 A global analysis of subsidence, relative sea-level change and coastal flood exposure, *Nat. Clim. Change*, 11, 338–342,
923 <https://doi.org/10.1038/s41558-021-00993-z>, 2021.

924 Papagiannaki, K., Petrucci, O., Diakakis, M., Kotroni, V., Aceto, L., Bianchi, C., Brázdil, R., Gelabert, M. G., Inbar, M.,
925 Kahraman, A., Kılıç, Ö., Krahn, A., Kreibich, H., Llasat, M. C., Llasat-Botija, M., Macdonald, N., de Brito, M. M., Mercuri,

926 M., Pereira, S., Řehoř, J., Geli, J. R., Salvati, P., Vinet, F., Zêzere, J. L.: Developing a large-scale dataset of flood fatalities for
927 territories in the Euro-Mediterranean region, *FFEM-DB, Sci. Data*, 9, 166, <https://doi.org/10.1038/s41597-022-01273-x>, 2022.

928 Paprotny, D. and Morales-Nápoles, O.: Estimating extreme river discharges in Europe through a Bayesian network, *Hydrol.*
929 *Earth Syst. Sci.*, 21, 2615-2636, doi:10.5194/hess-21-2615-2017, 2017

930 Paprotny, D., Mengel, M.: Population, land use and economic exposure estimates for Europe at 100 m resolution from 1870
931 to 2020, *Sci. Data*, 10, 372, <https://doi.org/10.1038/s41597-023-02282-0>, 2023.

932 Paprotny, D., Morales Nápoles, O., Nikulin, G.: Extreme sea levels under present and future climate: a pan-European database,
933 *E3S Web of Conferences*, 7, 02001, <https://doi.org/10.1051/e3sconf/20160702001>, 2016.

934 Paprotny, D., Morales Nápoles, O., Vousdoukas, M. I., Jonkman, S. N., and Nikulin, G.: Accuracy of pan-European coastal
935 flood mapping, *J. Flood Risk Manag.*, 12(2), e12459, <https://doi.org/10.1111/jfr3.12459>, 2019.

936 Paprotny, D., Morales-Nápoles, O., and Jonkman, S. N.: Efficient pan-European river flood hazard modelling through a
937 combination of statistical and physical models, *Nat. Hazards Earth Syst. Sci.*, 17, 1267–1283, [https://doi.org/10.5194/nhess-](https://doi.org/10.5194/nhess-17-1267-2017)
938 [17-1267-2017](https://doi.org/10.5194/nhess-17-1267-2017), 2017.

939 Paprotny, D., Morales-Nápoles, O., and Jonkman, S. N.: HANZE: a pan-European database of exposure to natural hazards and
940 damaging historical floods since 1870, *Earth Syst. Sci. Data*, 10, 565–581, <https://doi.org/10.5194/essd-10-565-2018>, 2018a.

941 Paprotny, D., Sebastian, A., Morales Nápoles, O., and Jonkman, S. N.: Trends in flood losses in Europe over the past 150
942 years, *Nat. Commun.*, 9, 1985, <https://doi.org/10.1038/s41467-018-04253-1>, 2018b.

943 Paprotny, D., Terefenko, P., and Śledziowski, J.: An improved database of flood impacts in Europe, 1870–2020: HANZE v2.1,
944 *Earth Syst. Sci. Data Discuss.* [preprint], <https://doi.org/10.5194/essd-2023-321>, in review, 2023.

945 Paprotny, D.: HANZE catalogue of modelled and historical floods in Europe, 1950-2020 [dataset],
946 <https://doi.org/10.5281/zenodo.10629443>, 2024.

947 [Paprotny D., t Hart C. M. P., Morales-Napoles O.: Evolution of flood protection levels and flood vulnerability in Europe since](#)
948 [1950 estimated with vine-copula models, Research Square \[preprint\], in review, https://doi.org/10.21203/rs.3.rs-4213746/v1,](#)
949 [2024.](#)

950 Peltier, W.R., Argus, D.F., and Drummond, R.: Space geodesy constrains ice-age terminal deglaciation: The global ICE-6G_C
951 (VM5a) model, *J. Geophys. Res. Solid Earth*, 120, 450-487, <https://doi.org/10.1002/2014JB011176>, 2015.

952 Poseidon System: Monitoring, forecasting and information system for the Greek seas, available at <https://poseidon.hcmr.gr/>.
953 Last accessed 16 January 2024.

954 ~~Pronk, M.: DeltaDTM: A global coastal digital terrain model. Version 1 [dataset], <https://doi.org/10.4121/21997565.v1>, 2023.~~

955 [Pronk, M., Hooijer, A., Eilander, D., Haag, A., de Jong, T., Vousdoukas, M., Vernimmen, R., Ledoux, H., Eleveld, M.:](#)
956 [DeltaDTM: A global coastal digital terrain model, Sci. Data, 11, 273, https://doi.org/10.1038/s41597-024-03091-9, 2024.](#)

957 Pujol, M.-I., Faugère, Y., Taburet, G., Dupuy, S., Pelloquin, C., Ablain, M., and Picot, N.: DUACS DT2014: the new multi-
958 mission altimeter data set reprocessed over 20 years, *Ocean Sci.*, 12, 1067–1090, <https://doi.org/10.5194/os-12-1067-2016>,
959 2016.

960 Rentschler, J., Avner, P., Marconcini, M., Su, R., Strano, E., Vousdoukas, M., and Hallegatte, S.: Global evidence of rapid
961 urban growth in flood zones since 1985, *Nature*, 622, 87–92, <https://doi.org/10.1038/s41586-023-06468-9>, 2023.

962 Rojas, R., Feyen, L., and Watkiss, P.: Climate change and river floods in the European Union: Socio-economic consequences
963 and the costs and benefits of adaptation. *Glob. Environ. Change*, 23, 1737–1751.
964 <https://doi.org/10.1016/j.gloenvcha.2013.08.006>, 2013.

965 Sauer, I., Reese, R., Otto, C., Geiger, T., Willner, S., Guillod, B. P., Bresch, D. N., and Frieler, K.: Climate signals in river
966 flood damages emerge under sound regional disaggregation. *Nat. Commun.*, 12, 2128, <https://doi.org/10.1038/s41467-021-22153-9>, 2021.

967 Schoppa, L., Barendrecht, M. H., Paprotny, D., Sairam, D., Sieg, T., and Kreibich, H.: Projecting Flood Risk Dynamics for
968 Effective Long-term Adaptation, *Earth's Future*, [12, e2022EF003258](https://doi.org/10.1029/2022EF003258), <https://doi.org/10.1029/2022EF003258>, ~~accepted in~~
969 ~~print~~, 2024.

970

971 Scussolini, P., Luu, L. N., Philip, S. Y., Berghuijs, W. R., Eilander, D., Aerts, J. C. J. H., Kew, S. F., van Oldenborgh, G. J.,
972 Toonen, W. H. J., Volkholz, J., Coumou, D.: Challenges in the attribution of river flood events, *WIREs Climate Change*, e874.
973 <https://doi.org/10.1002/wcc.874>, 2023.

974 Steinhausen, M., Paprotny, D., Dottori, F., Sairam, N., Mentaschi, L., Alfieri, L., Lüdtke, S., Kreibich, H., and Schröter K.:
975 Drivers of future fluvial flood risk change for residential buildings in Europe, *Global Environ. Chang.*, 76, 102559,
976 <https://doi.org/10.1016/j.gloenvcha.2022.102559>, 2022.

977 Taburet, G., Sanchez-Roman, A., Ballarotta, M., Pujol, M.-I., Legeais, J.-F., Fournier, F., Faugere, Y., and Dibarboue, G.:
978 DUACS DT2018: 25 years of reprocessed sea level altimetry products, *Ocean Sci.*, 15, 1207–1224, <https://doi.org/10.5194/os-15-1207-2019>, 2019.

979

980 Tellman, B., Sullivan, J. A., Kuhn, C., Kettner, A. J., Doyle, C. S., Brakenridge, G. R., Erickson, T. A., and Slayback, D. A.:
981 Satellite imaging reveals increased proportion of population exposed to floods, *Nature*, 596, 80–86,
982 <https://doi.org/10.1038/s41586-021-03695-w>, 2021.

983 Thiemig, V., Gomes, G. N., Skøien, J. O., Ziese, M., Rauthe-Schöch, A., Rustemeier, E., Rehfeldt, K., Walawender, J. P.,
984 Kolbe, C., Pichon, D., Schweim, C., and Salamon, P.: EMO-5: a high-resolution multi-variable gridded meteorological dataset
985 for Europe, *Earth Syst. Sci. Data*, 14, 3249–3272, <https://doi.org/10.5194/essd-14-3249-2022>, 2022.

986 Tilloy, A., Paprotny, D., Grimaldi, S., Gomes, G., Bianchi, A., Lange, S., Beck, H., and Feyen, L.: HERA: a high-resolution
987 pan-European hydrological reanalysis (1950–2020), *Earth Syst. Sci. Data Discuss.* [preprint], [https://doi.org/10.5194/essd-](https://doi.org/10.5194/essd-2024-41)
988 [2024-41](https://doi.org/10.5194/essd-2024-41), in review, 2024.

989 Treu, S., Muis, S., Dangendorf, S., Wahl, T., Oelsmann, J., Heinicke, S., Frieler, K., and Mengel, M.: Reconstruction of hourly
990 coastal water levels and counterfactuals without sea level rise for impact attribution, *Earth Syst. Sci. Data Discuss.* [preprint],
991 ~~<https://doi.org/10.5194/essd-2023-112>~~, ~~accepted in print, 2023.~~, [16, 1121–1136](https://doi.org/10.5194/essd-16-1121-2024), <https://doi.org/10.5194/essd-16-1121-2024>,
992 [2024](https://doi.org/10.5194/essd-16-1121-2024).

993 U.S. Army Corps of Engineers: Coastal Engineering Manual, EM 1110-2-1100, Department of the Army, Washington D.C.,
994 2002.

995 van der Knijff, J.: LISVAP– Evaporation Pre-Processor for the LISFLOOD Water Balance and Flood Simulation Model, User
996 Manual, Office for Official Publications of the European Communities, Luxembourg, <https://dx.doi.org/10.2788/26160>, 2006.

997 Vogt, J.V., Soille, P., De Jager, A., Rimaviciute, E., Mehl, W., Foisneau, S., Bodis, K., Dusart, J., Paracchini, M., Haastруп,
998 P., and Bamps, C.: A pan-European River and Catchment Database, Publications Office of the European Union, Luxembourg,
999 <https://dx.doi.org/10.2788/35907>, 2007.

1000 Vousdoukas, M. I., Athanasiou, P., Giardino, A., Mentaschi, L., Stocchino, A., Koop, R. E., Menéndez, P., Beck, M. W.,
1001 Ranasinghe, R., and Feyen, L.: Small Island Developing States under threat by rising seas even in a 1.5 °C warming world,
1002 *Nat. Sustain.*, <https://doi.org/10.1038/s41893-023-01230-5>, 2023.

1003 Vousdoukas, M. I., Mentaschi, L., Voukouvalas, E., Bianchi, A., Dottori, F., and Feyen, L.: Climatic and socioeconomic
1004 controls of future coastal flood risk in Europe, *Nat. Clim. Change*, 8, 776-780, <https://doi.org/10.1038/s41558-018-0260-4>,
1005 2018.

1006 Vousdoukas, M. I., Mentaschi, L., Voukouvalas, E., Verlaan, M., and Feyen, L.: Extreme Sea levels on the rise along Europe’s
1007 coasts, *Earth’s Future*, 5, 304–323, <https://doi.org/10.1002/2016ef000505>, 2017.

1008 Vousdoukas, M. I., Voukouvalas, E., Annunziato, A., Giardino, A., and Feyen, L.: Projections of extreme storm surge levels
1009 along Europe. *Climate Dynamics*, 47, 3171-3190, <https://doi.org/10.1007/s00382-016-3019-5>, 2016a.

1010 Vousdoukas, M. I., Voukouvalas, E., Mentaschi, L., Dottori, F., Giardino, A., Bouziotas, D., Bianchi, A., Salamon, P., and
1011 Feyen, L.: Developments in large-scale coastal flood hazard mapping, *Nat. Hazards Earth Syst. Sci.*, 16, 1841–1853,
1012 <https://doi.org/10.5194/nhess-16-1841-2016>, 2016b.

1013 Wada, Y., Flörke, M., Hanasaki, N., Eisner, S., Fischer, G., Tramberend, S., Satoh, Y., van Vliet, M. T. H., Yillia, P., Ringler,
1014 C., Burek, P., and Wiberg, D.: Modeling global water use for the 21st century: the Water Futures and Solutions (WFaS)
1015 initiative and its approaches, *Geosci. Model Dev.*, 9, 175–222, <https://doi.org/10.5194/gmd-9-175-2016>, 2016.

1016 Wing, O. E. J., Smith, A. M., Marston, M. L., Porter, J. R., Amodeo, M. F., Sampson, C. C., and Bates, P. D.: Simulating
1017 historical flood events at the continental scale: observational validation of a large-scale hydrodynamic model, *Nat. Hazards*
1018 *Earth Syst. Sci.*, 21, 559–575, <https://doi.org/10.5194/nhess-21-559-2021>, 2021.

1019 Zanaga, D., Van De Kerchove, R., De Keersmaecker, W., Souverijns, N., Brockmann, C., Quast, R., Wevers, J., Grosu, A.,
1020 Paccini, A., Vergnaud, S., Cartus, O., Santoro, M., Fritz, S., Georgieva, I., Lesiv, M., Carter, S., Herold, M., Li, Linlin,
1021 Tsendbazar, N.E., Ramoino, F., Arino, O.: ESA WorldCover 10 m 2020 v100 [dataset],
1022 <https://doi.org/10.5281/zenodo.5571936>, 2021.